AGU PUBLICATIONS

Paleoceanography

RESEARCH ARTICLE
10.1002/2014PA002643

Key Points:
- Brine formation is reconstructed for the deglaciation and Holocene periods
- Brine formation in Storfjorden, Svalbard is closely linked to climate
- Brines reached periodic maxima during the late Holocene (last circa 4000 years)

Correspondence to:
T. L. Rasmussen,
tine.rasmussen@uit.no

Citation:
Rasmussen, T. L., and E. Thomsen (2014), Brine formation in relation to climate changes and ice retreat during the last 15,000 years in Storfjorden, Svalbard, 76–78°N, *Paleoceanography*, *29*, 911–929, doi:10.1002/2014PA002643.

Received 20 MAR 2014
Accepted 11 SEP 2014
Accepted article online 15 SEP 2014
Published online 6 OCT 2014

Brine formation in relation to climate changes and ice retreat during the last 15,000 years in Storfjorden, Svalbard, 76–78°N

T. L. Rasmussen[1] and E. Thomsen[2]

[1]Centre for Arctic Gas Hydrate, Environment and Climate, Department of Geology, UiT The Arctic University of Norway, Tromsø, Norway, [2]Department of Geoscience, University of Aarhus, Aarhus, Denmark

Abstract Storfjorden, Svalbard, is an area of intense brine formation. The brine is cold, dense, rich in oxygen and CO_2, and has reduced pH. Storfjorden is unique because it contains well-preserved agglutinated foraminifera dating back to the beginning of the last deglaciation. We have investigated the distribution of calcareous and agglutinated benthic foraminifera, benthic oxygen and carbon isotopes, calcium carbonate, total organic carbon, and ice-rafted debris in five cores from Storfjorden comprising the Holocene and the deglaciation. The purpose of the study is to reconstruct brine formation in the past under different climate scenarios. The data indicate that in Storfjorden the ratio of agglutinated to calcareous benthic foraminifera can be taken as a measure of the strength of brine formation. The foraminiferal data, which are supported by stable isotopes, degree of fragmentation, and geochemical parameters, signify that brine formation intensified during cold periods and weakened during warm periods. During the deglaciation, increased brine flow coincides with the Older Dryas, the Intra-Allerød Cold Period, and the Younger Dryas. Brine formation increased from circa 8200 years B.P. reaching periodic maxima during the last 4000 years B.P. in response to the unstable climate. Maximum brine production correlates with the Dark Ages Cold Period circa 1500–1100 years B.P. and the Little Ice Age circa 600–100 years B.P. Lower production correlates with the Roman Warm Period circa 2500–2000 years B.P. and the Medieval Warm Period circa 1000–700 years B.P.

1. Introduction

Shelf brines provide about 10% of the deep water formed in the Arctic Ocean and Barents Sea today [*Smethie et al.*, 1986; *Quadfazel et al.*, 1988; *Rudels and Quadfasel*, 1991]. The major source of deep water is open ocean convection. Storfjorden, Svalbard, contributes about 5–10% of the brines [*Quadfazel et al.*, 1988; *Skogseth et al.*, 2004]. Brine formation is likely to have been equally important, or even more so, during the last glacial period, when the climate was much colder and the sea ice cover more extensive than at present. Conversely, during warm phases reduced sea ice probably led to a reduction in the ventilation by brines.

The present investigation focuses on the intense brine formation in Storfjorden, Svalbard [*Midttun*, 1985; *Quadfazel et al.*, 1988; *Schauer*, 1995; *Skogseth et al.*, 2004]. The brines are dense and have the potential to sink to at least 2 km water depth [*Quadfazel et al.*, 1988; *Schauer*, 1995]. Recent investigations indicate that brine production in Storfjorden varies with the North Atlantic Oscillation (NAO) index [*Skogseth et al.*, 2004]. The production is strongest in NAO winters, when the fjord is dominated by northeasterly winds and low temperatures, and weakest in NAO + winters, when southwesterly winds and higher temperatures take over. However, very little is known about brine formation in the Arctic in relation to climate changes on a longer time scale.

Brines carry CO_2-rich water into the deeper ocean, increasing the acidity of the deeper water masses [*Kelley*, 1968; *Anderson et al.*, 2004, 2010; *Omar et al.*, 2005; *Rysgaard et al.*, 2007; *Fransson et al.*, 2011]. The brine in Storfjorden has a high concentration of dissolved inorganic carbon and a lower pH than the surrounding water masses. Storfjorden is also very productive, and the content of organic matter in the sediments and suspended in the brine is high [*Anderson et al.*, 2004; *Winkelmann and Knies*, 2005; *Damm et al.*, 2007]. Some of the organic material is remineralized, thereby further increasing acidity of the brine [*Anderson et al.*, 1988; *Papadimitriou et al.*, 2003; *Delille et al.*, 2007; *Fransson et al.*, 2011; *Søgaard et al.*, 2013]. The brine may therefore affect the preservation of calcareous material and have an effect on the concentration of calcareous foraminifera [*Steinsund and Hald*, 1994].

©2014. American Geophysical Union. All Rights Reserved.

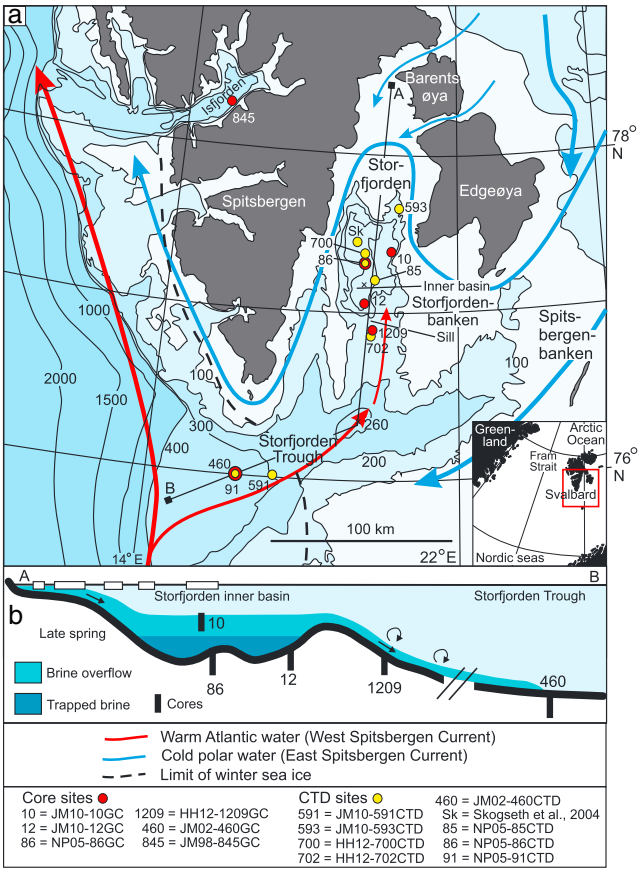

Figure 1. (a) Map of Storfjorden, Svalbard, showing position of cores (red circles) and CTD-stations (yellow circles). (b) North–south profile sketch of Storfjorden from the inner basin to shelf showing brine overflow. Core locations are indicated. Profile sketch is based on *Skogseth et al.* [2005b].

The purpose of this study is to investigate variations in brine formation in Storfjorden from the late glacial to recent in relation to climate changes. The study is based on five cores from the innermost brine basin to the shelf following the path of the brines from the inner fjord to the outer shelf (Figures 1a and 1b). Changes in brine formation are estimated on the basis of variations in the ratio of calcareous versus agglutinated benthic foraminiferal faunas, supplemented by the degree of fragmentation of benthic foraminifera, oxygen, and carbon isotopes measured on benthic foraminifera, the distribution of organic and inorganic carbon, and the occurrence of ice-rafted debris (IRD).

2. Oceanographic Setting

The archipelago of Svalbard stretches from ~ 76 to 80°N (Figure 1a). Storfjorden is a sound situated in the southeastern part of the archipelago between Spitsbergen to the west and Edgeøya and Barentsøya to the east. The West Spitsbergen Current carries warm Atlantic surface water northward along the western slope of Svalbard into the Arctic Ocean. Polar and Arctic surface water flow out of the Arctic Ocean east of Svalbard as the East Spitsbergen Current. The Arctic surface water enters Storfjorden via two sounds to the northeast and continues as a coastal current along the inner shelf of Svalbard (Figure 1a). A small branch of Atlantic surface water can enter Storfjorden from the south. In some years it can penetrate to the inner basin and mix with Arctic water [*Lydersen et al.*, 2002].

Storfjorden consists of an inner deep basin (maximum water depth ~190 m) flanked by a shallow shelf (<40 m water depth) to the north and northeast (Figures 1a and 1b). To the south, a 120 m deep sill separates the basin from Storfjorden Trough. During winter and spring, brines are formed on the shelf east of the deep basin [*Haarpainter et al.*, 2001; *Skogseth et al.*, 2008] (Figure 1b). The heavy water sinks and fills the basin, allowing the brine to overflow the sill. The overflow occurs from early spring (March–April) to summer (Figure 1b).

The intensity and property of the brines depend on strong winds from the northeast and the salinity of the surface water. The feed water is mainly the saline Arctic surface water from the Barents Sea, which enters via the two northeasterly sounds. The source water may have a contribution from high-salinity Atlantic water entering from the southwest during wintertime [*Schauer*, 1995; *Skogseth et al.*, 2005a, 2008]. The estimated outflow from the brine basin during the brine season amounts to 0.13 sverdrup (Sv) giving a year average of 0.06 Sv [*Rudels and Quadfasel*, 1991; *Schauer*, 1995; *Fer et al.*, 2003; *Skogseth et al.*, 2004].

Strong and cold winds from the northeast blow ice away from the eastern shelf and generate large polynya, where continuous freezing produces cold and salty brines (temperature < -1.9°C, salinity 34.8–35.8) [*Schauer*, 1995; *Haarpainter et al.*, 2001; *Anderson et al.*, 2004; *Skogseth et al.*, 2004, 2005a]. The largest brine

©2014. American Geophysical Union. All Rights Reserved.

production occurs during NAO winters, when winds from northeast predominate. Less brine is formed during NAO + winters dominated by southwesterly winds. In years with low surface salinity (<34.4) the brine are often too light to sink to deep water [*Schauer*, 1995; *Skogseth et al*., 2008].

The deepest part of the inner basin contains cold brine trapped year-round behind the sill. The temperatures are constantly below −1.0 to −1.5°C [*Fer et al*., 2003]. The brines have a lower pH than the surrounding water. *Anderson et al*. [2004], in the spring of 2002, measured a pH of ~7.83 at the bottom of the brine basin. This should be compared to a normal pH of >8.2 in the Atlantic water of the Nordic seas [e.g., *Feely et al*., 2009; *Chierici and Fransson*, 2009]. Polynyas are generally areas of high organic productivity [e.g., *Arrigo et al*., 2008], and Storfjorden is very productive compared to other areas of the Barents Sea. In Storfjorden the production of marine organic carbon may exceed 300 mgC cm^{-2} kyr^{-1}, while the production of total organic carbon (TOC) may exceed 500 mgC cm^{-2} kyr^{-1} [*Pathirana et al*., 2013].

3. Material and Methods

The investigation is based on four cores from Storfjorden. Three of the cores are from the inner brine basin, while one core is from the southern flank of the sill separating the brine basin from Storfjorden Trough (Figures 1a and 1b). In addition, we include published and unpublished data from a core from Storfjorden Trough on the outer shelf. The cores from the brine basin consist of NP05-86GC (350 cm long) taken at 142 m water depth [*Rasmussen and Thomsen*, 2009], JM10-10GC (402 cm long) taken at 123 m water depth in a subbasin below the western shelf of Edgeøya, and JM10-12GC (320 cm long) taken at 146 m water depth on the northern flank of the sill (Figures 1a and 1b). Core HH12-1209GC (267 cm long) from south of the sill was taken at 151 m water depth. The core from Storfjorden Trough JM02-460GC (387 cm long) was retrieved from a water depth of 389 m [*Rasmussen et al*., 2007]. The core sites outside the brine basin and core JM10-10GC from the eastern part of the basin are occasionally directly influenced by Atlantic water (Figures 1a and 2). In addition to these cores from Storfjorden we also present data from core JM98-845PC taken in Isfjorden at a water depth of 257 m [*Rasmussen et al*., 2012] (Figures 1a and 1b). Water property, temperature, salinity, and density were measured at or near all sites using a *Seabird 911 Plus* conductivity-temperature-depth (CTD). Data collection was performed during downcasts at a speed of approximately 1.0 m/s (Figure 2).

Magnetic susceptibility was measured in four cores. In JM10-10GC and JM10-12GC, the core was split and the magnetic susceptibility was measured on one core half using a handheld Bartington MS-2 point sensor at 2 cm intervals. In cores NP05-86GC and JM02-460GC, the susceptibility was measured before opening using a loop sensor mounted on a GEOTEK multisensor core logger.

Core NP05-86GC has previously been analyzed for the content of stable isotopes in benthic foraminifera [*Rasmussen and Thomsen*, 2009]. The same sample set, collected at 6 cm and 3 cm intervals, was used in this study. Cores JM10-10GC, JM10-12GC, and HH12-1209GC were split in two halves and one half of each core was cut up in 1 cm thick sample slices. The samples were wet weighed, freeze dried, and weighed again. Samples at 5 cm (core JM10-10GC) and 4 cm (cores JM10-12GC and HH12-1209GC) intervals were wet sieved over mesh sizes 63, 100, and 1000 μm and residues dried and weighed. The dry weight varies from ~ 25–35 g for samples of hemipelagic mud to 40–50 g for samples of glacimarine sediments. The size fraction >100 μm was analyzed for the content of benthic foraminifera. The same methods as in *Rasmussen et al*. [2007] were employed for the counts. The foraminifera were subdivided into agglutinated and calcareous forms, and the concentration of each group was calculated as the number of specimens per gram dry weight sediment. The percentages of agglutinated specimens were calculated relative to the total sum of calcareous and agglutinated specimens.

As a measure of preservation of the calcareous benthic foraminifera we calculated the percentage of fragmentation [e.g., *Berger et al*., 1982; *Conan et al*., 2002] in cores JM10-10GC and HH12-1209GC. The percentage was calculated as the number of fragments per gram dry weight sediment relative to the total number of whole specimens and fragments per gram dry weight sediment. For core HH12-1209GC, we used the >100 μm size fraction, while for core JM10-10GC we used the >150 μm size fraction. In core HH12-1209GC, the samples from the interval 93–155 cm (7500–11,700 years B.P.) are totally dominated by whole specimens and numerous fragments of *Nonionellina labradorica* and only 1–3% fragments of other species. *N. labradorica* is a fragile species, which easily breaks into many fragments. Because of the potential

©2014. American Geophysical Union. All Rights Reserved.

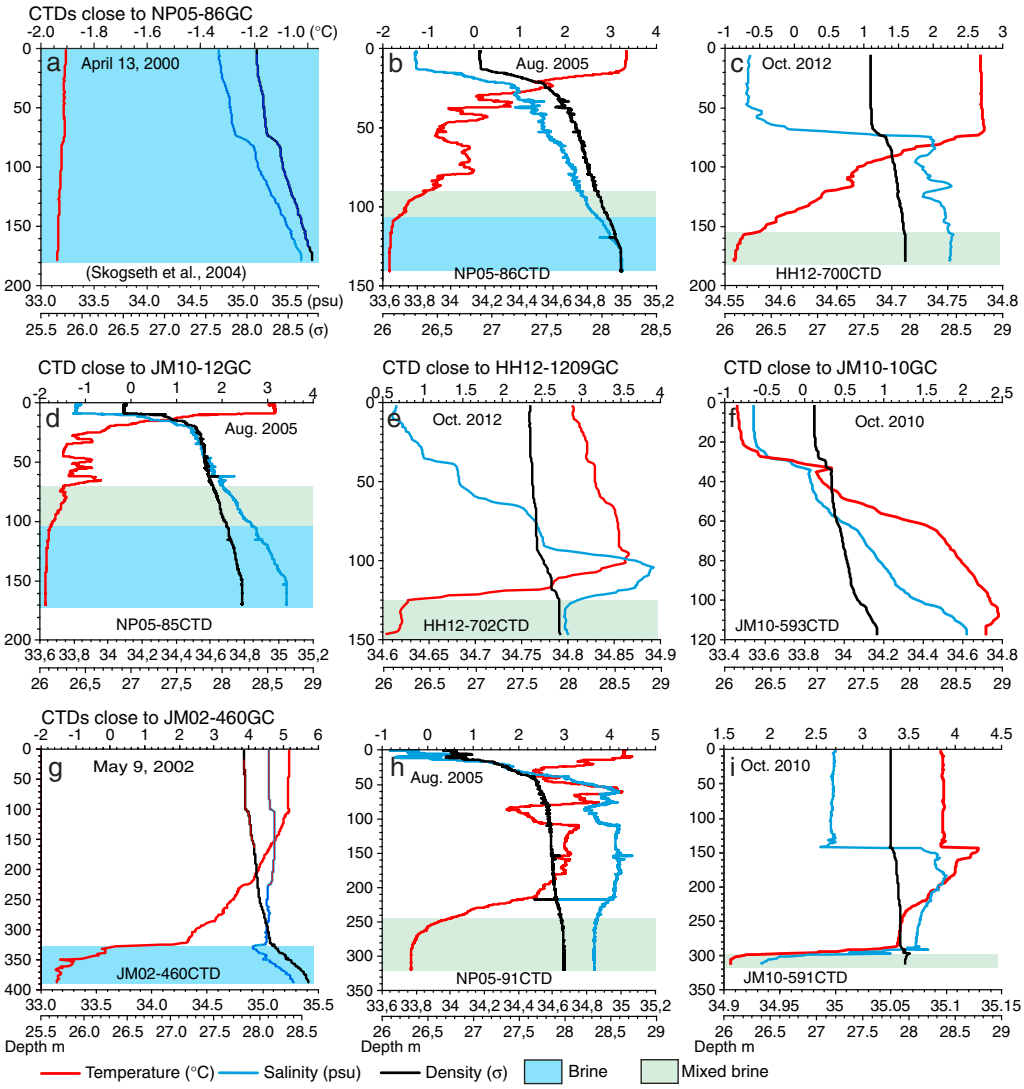

Figure 2. Conductivity, temperature, depth (CTD) plots from near or at core locations taken during years of strong brine formation (for exact location, see Figure 1a). The brine is generated by salt expulsion from continuous freezing of sea ice in polynya kept open by strong northeasterly winds. The properties of the brine vary from year to year depending on prevailing wind directions (see text for explanation). (a–c) CTD's from near core NP05-86GC. (d) CTD from near core JM10-12GC, (e) CTD from near core HH12-1209GC, (f) CTD from near core JM10-10GC. (g–i) CTD's taken at the position of core JM02-460GC. Note the very low temperatures of the bottom water in May (Figure 2g) and August (Figure 2h), when the brine was still cold and dense, as compared to the much higher bottom water temperatures in October (Figure 2i). Note also the strong pycnocline above the remains of the brine in October.

bias induced by fragmentation of *N. labradorica* [see *Le and Shackleton*, 1992; *Pfuhl and Shackleton*, 2004], we decided not to include counts from this interval.

In the three cores from the brine basin the residues were dry sieved over 500 μm sieves and the content of IRD was calculated as the number of mineral grains in the >500 μm grain size fraction per gram dry weight sediment. In core HH12-1209GC, IRD was counted in the size fraction >1 mm. In core JM02-460GC from Storfjorden Trough, we dry sieved previously studied samples [*Rasmussen et al.*, 2007] and used the >150 μm size fraction for counts of IRD (Figure 3).

In core JM10-12GC, stable isotopes were measured on well-preserved specimens without signs of dissolution of *N. labradorica*, *Cibicides lobatulus*, and *Cassidulina reniforme*. The former two species were corrected by oxygen isotope values of −0.2 and +0.64‰, respectively, to adjust for offsets between the various species

©2014. American Geophysical Union. All Rights Reserved.

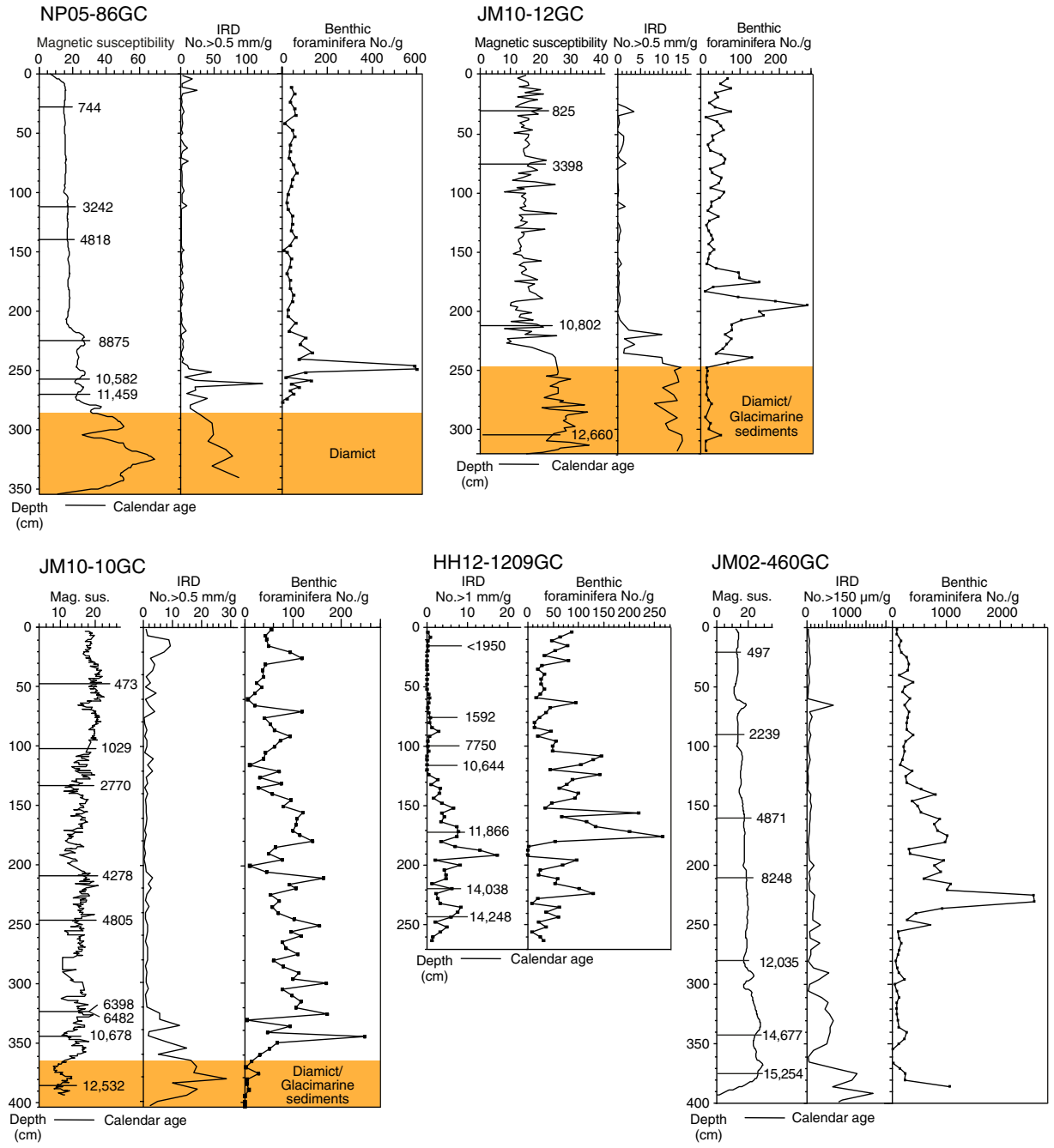

Figure 3. Magnetic susceptibility, concentration of ice rafted debris (IRD), and concentration of total (calcareous plus agglutinated) foraminifera (number per gram dry weight sediment) for each core (except for magnetic susceptibility in HH12-1209GC). Calibrated ages are marked in the magnetic susceptibility panels. The diamict or mixed diamitic/glacimarine deposits in the lower parts of the cores are indicated.

[see *Rasmussen and Thomsen*, 2009, and references therein]. The values of *C. reniforme* were not corrected (no offset; see *Hald et al*. [2004]). Previously published benthic isotope records of JM02-460GC (*C. lobatulus* and *Melonis barleeanus*) [*Rasmussen et al*., 2007] and NP05-86GC (*N. labradorica* and *C. lobatulus*} [*Rasmussen and Thomsen*, 2009] are included for comparison. The isotopes in core JM10-12GC were measured at the Bjerknes Centre, University of Bergen, while cores NP05-86GC and JM02-460GC were measured at Woods Hole Oceanographic Institution [see *Rasmussen and Thomsen*, 2009]. The results of the two laboratories are entirely compatible [*Jessen et al*., 2010; *Rasmussen et al*., 2014a]. The oxygen isotope values were corrected for ice volume changes [*Fairbanks*, 1989].

©2014. American Geophysical Union. All Rights Reserved.

Table 1. AMS14C Dates and Calibrated Dates for Cores JM10-10GC, JM10-12GC, NP05-86GC, HH12-1209GC, and JM02-460GC

Core	Depth (cm)	14C Age[a]	Calendar Age	Lab. Code	Species
JM10-10GC:	44.5	832 ± 21	473 ± 20	UB-17204	*Nucula sp.*
	102.5	1491 ± 22	1029 ± 43	UB-17205	*Nuculana sp.*
	136.5	3008 ± 27	2770 ± 32	UB-17206	*Astarte sp.*
	210.5	4182 ± 41	4278 ± 73	UB-18845	*N. labradorica*
	250.5	4573 ± 28	4805 ± 34	UB-18946	*N. labradorica*
	324–326	6065 ± 31	6482 ± 49	UB-17207	Bivalve
	325	5990 ± 43	6398 ± 57	UB-21198	*N. labradorica*
	345–346	9778 ± 40	10,678 ± 64	UB-18947	Bivalve
	385–386	10,960 ± 44	12,532 ± 55	UB-18948	Bivalve
JM10-12GC:	31.5	1275 ± 23	825 ± 43	UB-17208	*Portlandia arctica*
	75.5	3513 ± 27	3398 ± 36	UB-21669	Molluscs
	175.5	No data	No data	UB-21670	*N. labradorica*
	212–214	9970 ± 45	10,802 ± 90	UB-17209	*Nuculana*
	305–306	11,160 ± 81	12,660 ± 65	UB-21671	Foraminifera, molluscs
NP05-86GC:	28.5	1212 ± 32	744 ± 42	AAR-10854	*Cylichna spp.*
	110.5	3371 ± 39	3242 ± 61	AAR-10918	Gastropod
	140.5	4593 ± 46	4818 ± 48	AAR-10739	*Ophiura ossicles*
	224.5	8305 ± 50	8875 ± 88	AAR-10919	*Nucula sp.*
	257.5	9685 ± 55	10,582 ± 69	AAR-10740	*N. labradorica*
	269.5	10,395 ± 60	11,459 ± 156	AAR-10920	*Nuculana sp.*
HH12-1209GC	15.5	>modern	<1950 A.D	UB-24643	*Thyasira sp.*
	75.5	2034 ± 25	1592 ± 45	UB-24644	*Portlandia arctica*
	99.5	6894 ± 37	7750 ± 50	UB-25883	*Nucula sp.*
	127.5	9750 ± 48	10,644 ± 65	UB-24645	*Nucula sp.*
	171.5	10,568 ± 43	11,866 ± 106	UB-24646	*Nuculana sp.*
	219.5	12,953 ± 53	14,038 ± 76	UB-24647	*Thyasira sp.*
	243.5	13,105 ± 66	14,248 ± 157	UB-25612	Foraminifera, molluscs
JM02-460GC:	20	880 ± 55	497 ± 41	AAR-8915	Bivalve
	90	2570 ± 60	2239 ± 74	AAR-8916	Foraminifera
	160	4645 ± 50	4871 ± 57	Tua-3975	Bivalves
	210	7780 ± 65	8248 ± 69	AAR-8917	Benthic foraminifera
	280	10,655 ± 140	12,035 ± 299	Tua-3976	Foraminifera, molluscs
	340-345	12,890 ± 110	14,677 ± 287	AAR-8918	Bivalve, gastropod
	375	13,180 ± 140	15,254 ± 254	Tua-3977	Bivalve

[a]Conventional ages.

In cores NP05-86GC and JM02-460GC, bulk samples taken at 4 cm and 2 cm intervals, respectively, were analyzed for the content of total carbon (%TC), total organic carbon (%TOC), and calcium carbonate (%$CaCO_3$) using a Leco CS-200 induction furnace. The weight percentage of $CaCO_3$ (wt %) was calculated as follows: $\%CaCO_3 = (TC - TOC) \times 100/12$.

A total of 26 AMS ^{14}C dates have been obtained from cores NP05-86GC (six dates including three previously published dates), JM10-10GC (nine dates), JM10-12GC (five dates), and HH12-1209GC (seven dates). The datings of NP05-86GC were performed at the AMS-Dating Centre, University of Aarhus, Denmark. The other samples were dated at the ^{14}CHRONO Centre at Queen's University Belfast (Table 1). The seven dates from core JM02-460GC are published in *Rasmussen et al.* [2007]. All AMS ^{14}C dates were calibrated to calendar age applying the Calib7.01 and the Marine13 program [*Stuiver and Reimer*, 1993; *Reimer et al.*, 2013] (Table 1). The midpoint of the calibrated ages ($\pm 1\sigma$) was chosen. The ages mentioned below are in calendar years unless otherwise indicated.

4. Results

4.1. Lithology, Sedimentation Rates, and Construction of the Age Models

Lithologically, cores JM10-10GC, JM10-12GC, and HH12-1209GC are similar. They consist of a thick unit of black and brownish homogeneous, marine mud overlying a unit of coarse sediment (Figure 3). Core JM05-86GC consists of black homogenous mud on top of unsorted gravel in a matrix of dark, sandy mud devoid of foraminifera and

©2014. American Geophysical Union. All Rights Reserved.

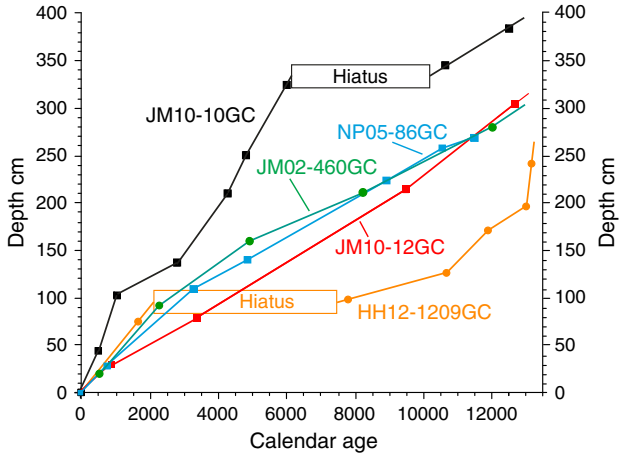

Figure 4. Age-depth plot for the five investigated cores.

macrofauna. The lower unit is interpreted as a diamict in core NP05-86GC and as a mixture of diamictic and glacimarine deposits in cores JM10-10GC, JM10-12GC, and HH12-1209GC. JM02-460GC from Storfjorden Trough consists entirely of dark, greenish-gray mud [*Rasmussen et al.*, 2007].

An age model was calculated for the strictly marine section of each core by adopting linear sedimentation rates between dating points (Figure 4). In all cores, we assume that the core tops are recent. The sedimentation rates of cores NP05-86GC and JM10-12GC are relatively uniform averaging 23.5 and 24 cm/ka, respectively. In both cores, the rate increases upward to a maximum of 38 cm/ka in the upper part (Figure 4). However, we were only able to obtain a few dates in core JM10-12GC and the age model for the upper part of this core is probably slightly misleading. The sedimentation rates of cores JM10-10GC and HH12-1209GC are more variable. In JM10-10GC, the rate ranges from 104 cm/ka in the upper part to 19–20 cm/ka in the middle part (Figure 4). The sedimentation rate calculated for the interval between 324.5 cm and 345.5 cm is extremely low, indicating the presence of a hiatus. A bivalve sampled at 324.5 cm was dated to circa 6000 years (Table 1 and Figure 3), while a foraminiferal sample from 345.5 cm gave an age of 10,680 years. The bivalve could have been misplaced downward due to burrowing or during the coring procedure, but the dating was confirmed by a new dating based on a monospecific sample of the benthic foraminiferal species *N. labradorica* (Table 1 and Figure 3). The time span of the hiatus is estimated to 6500–9500 years B.P. by accepting the sedimentation rates calculated for the intervals immediately above and below the hiatus (Table 1 and Figure 4). In core HH12-1209GC, a low sedimentation rate in combination with a lithological shift and an abrupt change in the foraminiferal faunas indicate the presence of a hiatus at 95.5 cm downcore. The time span of the hiatus is calculated to circa 7500–2000 years B.P. following the principles described above for core JM10-10GC.

A sample taken about 10 cm above the diamict in core NP05-86GC is dated to 11,460 years (Figures 3 and 4, and Table 1). By extending the sedimentation rate calculated for the interval between the lowermost two dates we obtain an age of circa 11,600 years B.P. for the base of the marine mud. This age is close to the age of the start of the Holocene as defined in the Greenland ice cores [*Rasmussen et al.*, 2006]. Using the same methods, the bottom of core HH12-1209GC is dated to circa 14,500 years B.P. (Figures 3 and 4, and Table 1). In cores JM10-12GC, JM10-10GC, and HH12-1209GC, the lower parts interpreted to be a diamict or a mixture of diamict and glacimarine sediments contain foraminifera and in some levels in sufficient amounts for ^{14}C datings (Table 1). Thus, a sample from near the bottom of core JM10-10GC is dated to 12,532 years B.P., while a sample from the lowermost part of JM10-12GC is dated to 12,660 years B.P.

4.2. Distribution of Benthic Foraminifera, IRD, TOC, $CaCO_3$, and Stable Isotopes

In the records from the brine basin we are mainly concerned only with the well-dated marine deposits younger than circa 11,700 years B.P. (Figures 3, 4, and 5a). Core HH12-1209GC from the southern flank of the sill and core JM02-460GC from Storfjorden Trough reach farthest back in time comprising the last circa 15,000 years and including the Bølling and Allerød interstadials, the Younger Dryas stadial, and the Holocene interglacial [*Rasmussen et al.*, 2007] (Figures 3, 4, and 5b). Since we are using independent age models, ages of apparently matching events can be expected to deviate slightly from core to core due to uncertainties in reservoir age corrections, various dating errors, and changes in sedimentation rates (see discussion in *Rasmussen et al.* [2014b]) (Figure 3 and Table 1).

The distribution patterns of calcareous and agglutinated benthic foraminifera from the Holocene intervals of the five records have many characteristic features in common and have fairly similar timing (Figures 5a, 5b,

©2014. American Geophysical Union. All Rights Reserved.

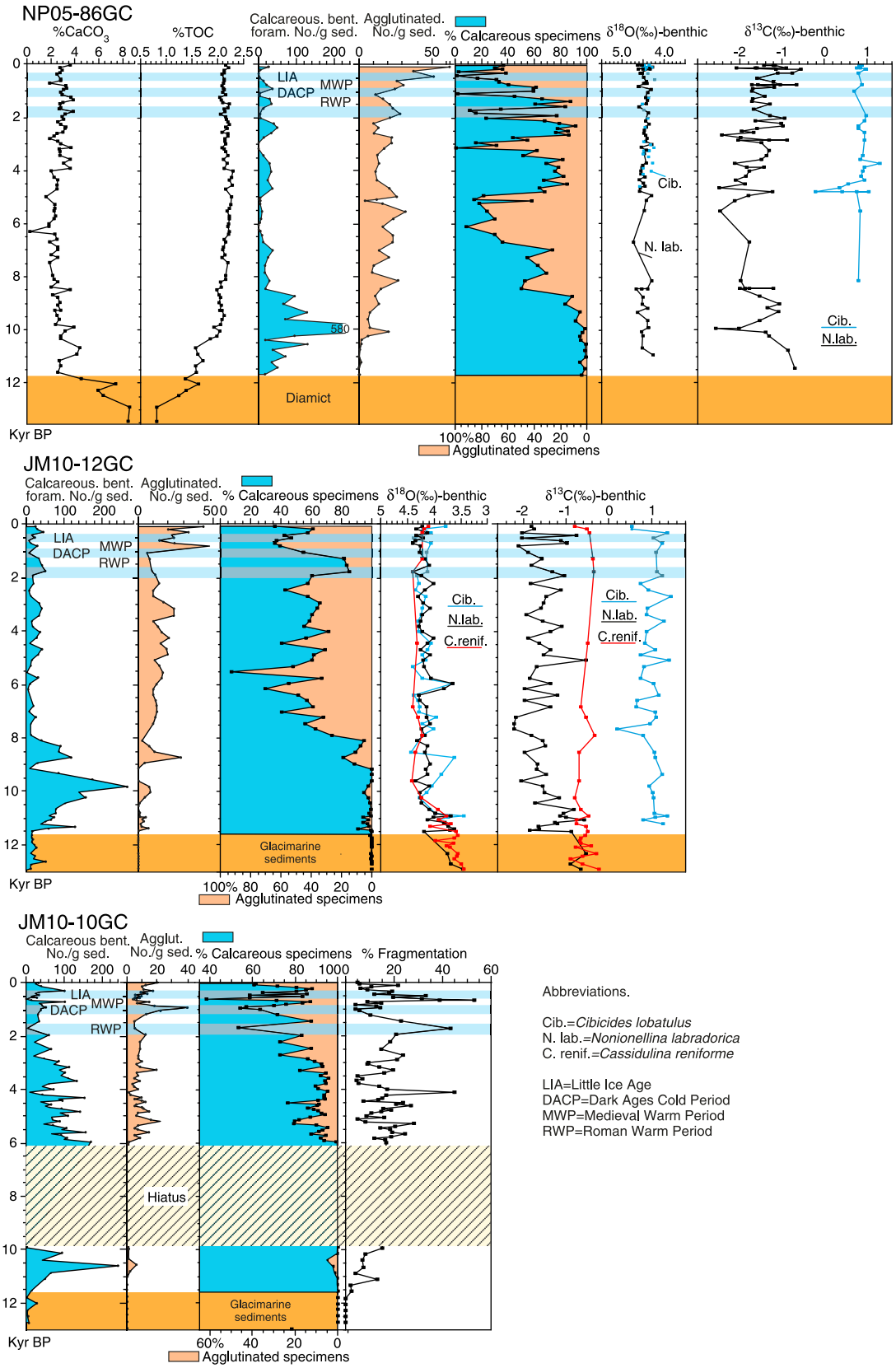

Abbreviations.

Cib.=*Cibicides lobatulus*
N. lab.=*Nonionellina labradorica*
C. renif.=*Cassidulina reniforme*

LIA=Little Ice Age
DACP=Dark Ages Cold Period
MWP=Medieval Warm Period
RWP=Roman Warm Period

Figure 5

©2014. American Geophysical Union. All Rights Reserved.

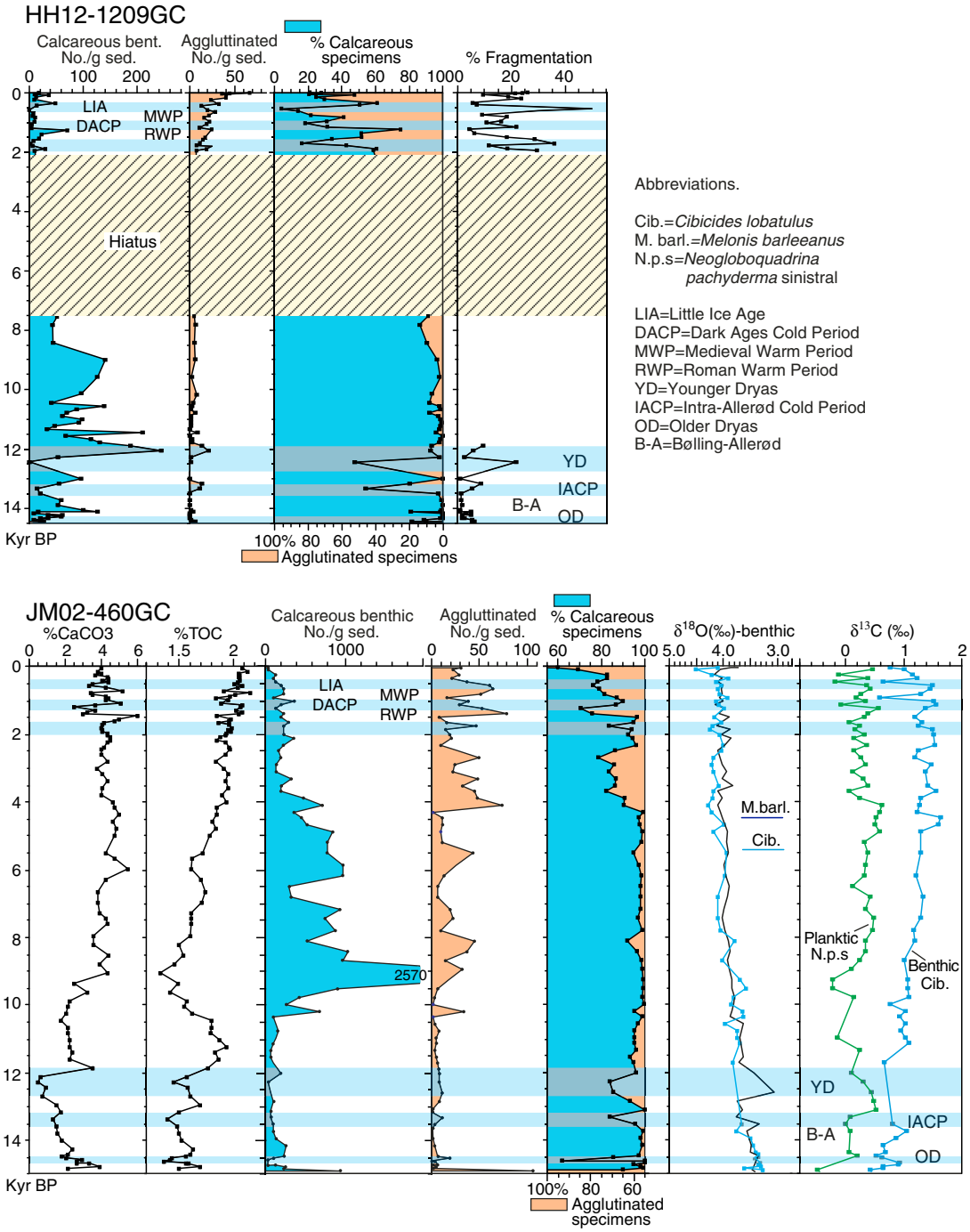

Figure 5. (continued)

and 6). In all cores, agglutinated forms are absent or very rare in Holocene deposits older than circa 9000–10,000 years B.P. (Figures 5a and 5b). They are nearly constant in absolute abundance from circa 9000 years B.P. until the last circa 1000 years, when they increase. In cores NP05-86GC and JM10-12GC from the brine basin the relative abundance of agglutinated specimens increases from circa 8500, and they are dominating from about 8200–5000 years B.P., when they often make up 60–80% of the benthic faunas (Figures 5a and 6). The increase is much smaller in core JM02-460GC, where the relative abundance of agglutinated foraminifera remains low until circa 4000 years B.P. The upper part of the records younger

©2014. American Geophysical Union. All Rights Reserved.

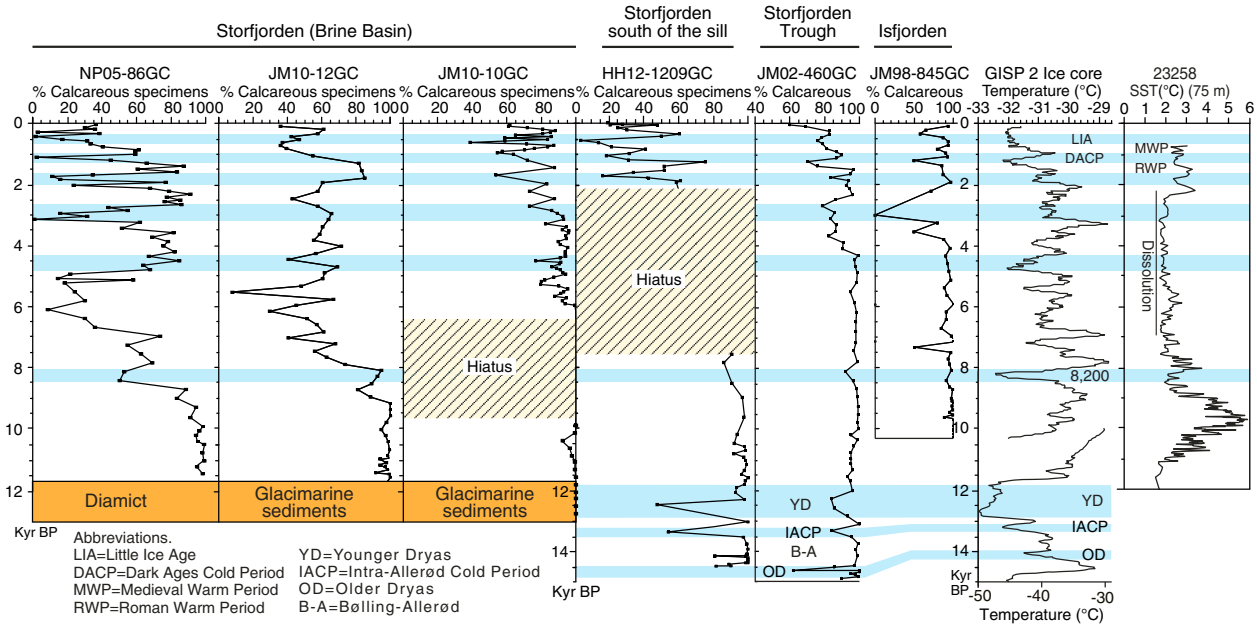

Figure 6. Plot of relative abundances of calcareous and agglutinated specimens for the five cores and JM98-845PC (data from *Rasmussen et al.* [2012]) along the $\delta^{18}O$ values of GISP2 ice core (data from *Cuffey and Clow* [1997] and *Alley* [2000]) and a sea surface temperature record from core 23258 (data from *Sarnthein et al.* [2003]). Blue bars mark cold events with high relative abundance of agglutinated specimens and increased percentage of fragmentation.

than circa 4–3000 years are in all five cores, characterized by strongly fluctuating proportions of calcareous and agglutinated specimens.

The deglaciation, as represented in JM02-460GC from Storfjorden Trough and in HH12-1209GC from south of the sill, is distinguished by three distinct maxima of agglutinated forms correlating in age with the Older Dryas (OD; centered at 14,600 years B.P. [*Stanford et al.*, 2006]), the Intra-Allerød Cold Period (IACP; centered at 13,300 years B..P [*Björck et al.*, 1996]), and the Younger Dryas events (YD; 12,900–11,700 years B.P. [*Rasmussen et al.*, 2006]) as these periods are dated in marine and terrestrial records (Figures 5b and 6).

The agglutinated foraminifera are generally of bright red coloration, indicating that their cement contains iron in an oxygenated state [*Hedley*, 1963; *Commeau et al.*, 1985; *Loeblich and Tappan*, 1989; *Gooday and Claugher*, 1989]. For all cores, we find that the preservation of calcareous foraminifera ranges from good to excellent in the deposits older than circa 8200 years. This is also reflected in the percentage of fragmentation, which is relatively low in deposits older than 10,000 years B.P., although with distinct increases in the intervals referred to the Younger Dryas, the Intra-Allerød Cold Period. and the Older Dryas (Figures 5a and 5b). Due to the presence of hiatuses in cores HH12-1209GC and JM10-10GC, we have no data for the mid-Holocene interval (Figures 5a and 5b). After 6000 years B.P., the percentage of fragmentation increases and becomes more fluctuating. From circa 3500 years B.P., during

Figure 5. (a) Data from the five cores plotted versus calendar years B.P. (top row) Core NP05-86GC showing percentage of $CaCO_3$, percentage of TOC, number of calcareous benthic foraminifera per gram dry weight sediment (dwt sed), number of agglutinated benthic foraminifera per dwt sed, relative abundance of calcareous and agglutinated specimens, and oxygen isotopes and carbon isotopes measured in *N. labradorica* (black) and *Cibicides lobatulus* (blue). (middle row) Core JM10-12GC showing number of calcareous benthic foraminifera per dwt sed, number of agglutinated benthic foraminifera per dwt sed, relative abundance of calcareous and agglutinated specimens, and oxygen and carbon isotopes measured in *N. labradorica* (black), *Cibicides lobatulus* (blue), and *Cassidulina reniforme* (red). (bottom row) Core JM10-10GC showing number of calcareous benthic foraminifera per dwt sed, number of agglutinated benthic foraminifera per dwt sed, relative abundance of calcareous and agglutinated specimens, and percentage fragmentation in the size fraction >150 μm. (b) (top row) Core HH12-1209GC showing number of calcareous benthic foraminifera per dwt sed, number of agglutinated benthic foraminifera per dwt sed, relative abundance of calcareous and agglutinated specimens, and percentage of fragmentation in the size fraction >100 μm. (bottom row) Core JM-460GC showing percentage $CaCO_3$, percentage TOC, number of calcareous benthic foraminifera per dwt sed, number of agglutinated benthic foraminifera per dwt sed, relative abundance of calcareous and agglutinated specimens, and oxygen isotopes and carbon isotopes measured in *Melonis barleeanus* (dark blue), *Cibicides lobatulus* (blue), and planktic foraminifera *Neogloboquadrina pachyderma* s (green, ^{13}C only). Stable isotope data for cores NP05-86GC and JM02-460GC are from *Rasmussen et al.* [2007] and *Rasmussen and Thomsen* [2009]. Blue bars mark events with high relative abundance of agglutinated specimens and increased percentage of fragmentation.

©2014. American Geophysical Union. All Rights Reserved.

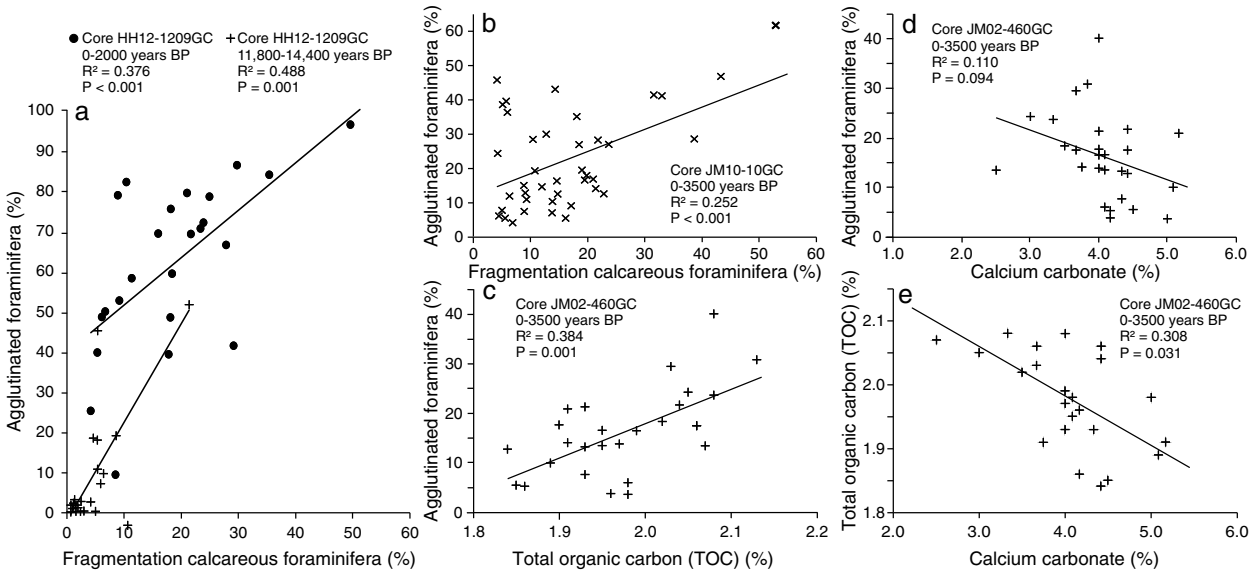

Figure 7. (a) Scatterplot of percentage of fragmentation against percentage of agglutinated foraminifera for cores HH-1209GC. The late Holocene and deglaciation periods are analyzed separately as they represent distinctly different ecological and preservational conditions. (b) Scatterplot of percentage of fragmentation against percentage of agglutinated foraminifera for the last 3500 years of core JM10-10GC. (c) Scatterplot of percentage of total organic carbon (TOC) against percentage of agglutinated foraminifera for the last 3500 years of core JM02-460GC. (d) Scatterplot of percentage of calcium carbonate against percentage of agglutinated foraminifera for the last 3500 years of core JM02-460GC. (e) Scatterplot of percentage of total organic carbon (TOC) against percentage of calcium carbonate for the last 3500 years of core JM02-460GC. Raw data for each panel are plotted in Figures 5a and 5b. Regression line and statistical data (R^2 values and P values) are indicated for each panel. The P values indicate that all correlations are significant, except for the correlation of percentage of calcium carbonate against percentage of agglutinated foraminifera (Figure 7c).

the deglaciation, there is a clear positive correlation between maxima in percentage of fragmentation and peaks in the relative abundance of agglutinated foraminifera (Figures 5a, 5b. and 7).

TOC was only measured in NP05-86GC from the brine basin and in JM02-460GC from Storfjorden Trough (Figures 5a and 5b). In NP05-86GC, the content of TOC is low in the diamict, increasing to >2% in the marine deposits (Figure 5a). The percentage of $CaCO_3$ shows the opposite trend. In core JM02-460GC, the percentage of TOC is high in the interval from circa 11,700 to circa 10,000 years B.P. and low from 10,000 to 8200 years B.P., after which the values gradually increase to a maximum >2% in the upper part. In the section younger than circa 3500 years B.P. the values are highly variable with high percentages of TOC correlating with high percentages of agglutinated foraminifera (Figures 5b and 7). The percentages of $CaCO_3$ show the opposite trend of the TOC percentages during the early Holocene. From 8000 years B.P. to recent, the values have been relatively stable although with increasing fluctuations during the late Holocene after circa 3500 years B.P. In the late Holocene interval of core JM02-460GC, we notice a weak, not statistically significant, negative correlation between the percentages of $CaCO_3$ and the relative abundances of agglutinated specimens (Figures 5b and 7). In the deglacial deposits, the content of TOC and $CaCO_3$ is low with three distinct minima in the TOC percentages correlating with the cold OD, IACP, and YD events and with higher relative abundance of agglutinated specimens (Figure 5b).

The oxygen isotope values are highest in core NP05-86GC from the deepest part of the brine basin (Figure 5a). The values are slightly lower in core JM10-12GC and lowest in core JM02-460GC from the trough. In core NP05-86GC, the values are nearly constant throughout the record, whereas in core JM02-460GC they are gradually increasing (Figures 5a and 5b). The $\delta^{13}C$ values measured in *C. lobatulus* in cores NP05-86GC and JM10-12GC from the brine basin shows little variability, although there seems to be a slight minimum from circa 8000 to 6000 years B.P. This minimum can also be seen in the general trends recorded on the endobenthic species *N. labradorica* (Figure 5a). In core JM02-460GC, the values have been slightly increasing throughout the last 15,000 years.

©2014. American Geophysical Union. All Rights Reserved.

5. Discussion

The concentration of agglutinated and calcareous foraminifera and the percentage ratio of the two groups vary significantly both geographically and through time (Figures 5a, 5b, and 6). However, the ratio shows basically the same trend in all five cores. In the first part of this discussion we will examine possible explanations for the shifting ratio of agglutinated to calcareous benthic foraminifera.

5.1. Environmental Factors Affecting the Ratio of Agglutinated to Calcareous Benthic Foraminifera

5.1.1. The Distribution of Agglutinated Foraminifera on the Shelf Around Svalbard

Predominance of agglutinated foraminifera is normally associated with difficult environmental conditions, where the more adaptable agglutinated species can gain an advantage over the calcareous species, and with acidic environments, where calcareous tests may be dissolved [*Steinsund and Hald*, 1994; *Murray and Alve*, 1999, 2011; *Alve et al*., 2011]. However, agglutinated foraminifera generally have a poor preservation potential and most species disintegrate soon after death. A few species may survive a little longer, but agglutinated specimens are usually rare or absent in Quaternary sediments below the uppermost ~30 cm of the sea bottom [e.g., *Sidner and McKee*, 1975; *Schröder*, 1988; *Denne and Sen Gupta*, 1989; *Wollenburg and Kuhnt*, 2000; *Kuhnt et al*., 2000].

Most sediment cores from the western and northwestern margin of Svalbard follow this typical pattern [see *Cadman*, 1996; *Ślubowska et al*., 2005; *Ślubowska-Woldengen et al*., 2007; *Skirbekk et al*., 2010; *Kubischta et al*., 2011]. The cores from Storfjorden are exceptional by preserving a high, although fluctuating, percentage of agglutinated specimens from top to bottom. In addition to the cores from Storfjorden, agglutinated foraminifera are only common in core JM98-845GC from Isfjorden [*Rasmussen et al*., 2012] and in a core from northeast of Svalbard, where they occur in low abundance [*Klitgaard Kristensen et al*., 2013]. In both of these areas the bottom water is affected by brines [*Nilsen et al*., 2008; *Lubinski et al*., 2001].

In recent faunas from the shelf of Svalbard and the Barents Sea, the percentage of agglutinated foraminifera varies from $<$25% to $>$75% [*Steinsund*, 1994; *Korsun and Hald*, 1998]. The lowest percentages are typically found west and south of Svalbard in areas influenced by Atlantic water, while the highest percentages are found to the east and north in areas dominated by Arctic water. The main factors responsible for the low proportion of calcareous specimens east and north of Svalbard is carbonate dissolution due to the presence of CO_2-rich brine at the bottom and/or a high content of organic carbon in the sediments and bottom water [*Hald and Steinsund*, 1992, 1996; *Steinsund*, 1994; *Steinsund and Hald*, 1994]. Fossil faunas dominated by agglutinated foraminifera are often the remnants after the calcareous faunas have been dissolved [*Alve and Murray*, 1995]. This indicates that the absence of agglutinated specimens in most cores and their presence inthe cores from Storfjorden and Isfjorden are primarily controlled by preservational factors. This is supported by the high degree of fragmentation in periods dominated by agglutinated foraminifera (Figures 5a, 5b, and 7).

The correlation between water masses and the ratio of agglutinated to calcareous foraminifera seen on the western slope of Svalbard is in good agreement with numerous observations of the preservation of the two groups in Arctic and sub-Arctic Oceans. Areas under the influence of Atlantic water tends to have a good preservation of calcium carbonate [e.g., *Hebbeln and Berner*, 1993; *Hebbeln et al*., 1998; *Scott et al*., 2008; *Schröder-Adams and van Rooyen*, 2011], whereas areas influenced by cold Polar/Arctic/Antarctic water or by brines tend to have poor preservation [*Steinsund and Hald*, 1994; *Hald and Steinsund*, 1996; *Ishman and Foley*, 1996; *Li et al*., 2000; *Belyaeva and Burmistrova*, 2003]. Furthermore, areas with poor preservation of calcareous specimens show often good preservation and predominance of agglutinated specimens [*Anderson*, 1975a, 1975b; *Mackensen et al*., 1990; *Murray and Alve*, 1999; *Li et al*., 2000; *Murray*, 2003; *Wollenburg and Kuhnt*, 2000; *Wollenburg et al*., 2007; *Schell et al*., 2008; *Alve et al*., 2011].

5.1.2. Factors Affecting the Distribution of Agglutinated and Calcareous Foraminifera Around Svalbard and in the Arctic Ocean

There are several factors that can influence the differential preservation of calcareous and agglutinated foraminifera in cold Arctic environments. The most important are the following: CO_2 content (pH), temperature, salinity, oxygenation, content and productivity of organic material and remineralization of same, and sedimentation rate.

©2014. American Geophysical Union. All Rights Reserved.

The well-preserved agglutinated specimens in Storfjorden and Isfjorden are generally tinted red, indicating that their cement contains ferruginous material in an oxygenated state (see above). Agglutinated foraminifera with cement containing iron preserve best in oxidized environments and tend to disintegrate under reducing conditions [*Sidner and McKee*, 1975; *Schröder*, 1986, 1988; *Gooday*, 1994]. The longer these types of agglutinated tests are exposed to oxygenated conditions the better the chance is for preservation (see discussion in *Korsun and Hald* [1998, and references therein]). The situation for calcareous foraminifera is the opposite. Long-time exposure to oxidized conditions at the sediment surface (together with burrowing activities) increases the degree of dissolution of calcium carbonate [*Loubere and Gary*, 1990; *Korsun and Hald*, 1998]. The faster a calcareous test is buried and transferred to reducing conditions the better the chance is for preservation. Furthermore, lower temperature, higher CO_2 content, lower pH, and higher salinity increase the corrosiveness of water to calcium carbonate [e.g., *Mackensen and Douglas*, 1989; *Mackensen et al.*, 1990; *Hald and Steinsund*, 1996; *Majewski and Zajączkowski*, 2007]. With their high content of oxygen and CO_2, low pH, and very low temperatures, the brines in Storfjorden are very corrosive to calcareous foraminifera, but at the same time they act to better preserve the agglutinated forms (with a ferruginous type of cement).

There are, however, a number of other factors that may affect the preservation of foraminifera in the Arctic. High organic productivity and a high content of organic material in the sediments and in the bottom water can increase the acidity of the bottom environment and cause dissolution in calcareous tests [e.g., *Walter and Burton*, 1990]. In the Nordic seas and in the Arctic Ocean, high productivity occurs characteristically at the sea ice edge and near the Arctic Front [*Johannessen*, 1987; *Smith et al.*, 1985; *van Aken et al.*, 1991; *Wollenburg and Kuhnt*, 2000; *Wassmann et al.*, 2006; *Wollenburg et al.*, 2007; *Reigstad et al.*, 2011]. In Storfjorden the production of marine organic carbon is very high and correlated with the duration of the seasonal sea cover [*Winkelmann and Knies*, 2005; *Pathirana et al.*, 2013]. Polynyal activity may further increase the primary productivity [e.g., *Arrigo et al.*, 2008] accentuating the acidity of the bottom water. In warmer periods the sea ice season is shorter and the organic productivity is reduced. The marine organic production is supplemented by organic material of terrestrial origin, and the content of TOC in the Holocene sediments of the brine basin is high [*Winkelmann and Knies*, 2005] (see also Figure 5a).

The sedimentation rate may also exert an influence on the preservation of benthic foraminifera. High sedimentation rates generally promote the preservation of calcium carbonate and demote the preservation of ferrigenous agglutinated tests, and vice versa for low sedimentation rates (see above). Other types of agglutinated foraminifera may preserve better if they are buried rapidly below the redox boundary [*Murray and Alve*, 2011, and references therein]. However, in Storfjorden, the sedimentation rate is different from record to record (Figure 4), and the degree of variability between the records also differs. Yet the distribution patterns of agglutinated versus calcareous species are similar (Figures 5a, 5b, and 6). The timing of changes is also fairly similar. The sedimentation rate has therefore probably played only a minor role for the observed preservational patterns as compared to brine formation and organic productivity.

Based on these modern observations we conclude that the intensity of brine formation most likely was the main factor responsible for the changes in the ratio of agglutinated to calcareous benthic foraminifera in Storfjorden during the last 15,000 years, possibly supplemented by changes in organic productivity, which often operates in concert with brine formation. Brines have a high content of CO_2 and organic substances and a low pH; factors that act to dissolve $CaCO_3$ [*Anderson et al.*, 2004]. Brines are also rich in oxygen, which can promote the preservation of ferrigenous agglutinated specimens. This indicates that the ratios of agglutinated to calcareous foraminifera in Storfjorden can be taken as an indication of changes in brine formation in the past.

5.2. Brine Formation in Storfjorden in Relation to Climate Changes and Ice Retreat

The Svalbard ice sheet retreated from the site of core JM02-460GC on outer shelf of Storfjorden before 19,700 years B.P. [*Rasmussen et al.*, 2007] (Figure 8a). The oldest marine sediments in core HH12-1209GC from the southern flank of the sill dates from the Bølling interstadial 14,500 years B.P. (Figure 3). In core NP05-86GC from the inner brine basin, the oldest marine sediments above the diamict are assigned to shortly after the start of the Holocene [*Rasmussen and Thomsen*, 2009] (Figure 3 and Table 1). In cores JM10-10GC and JM10-12GC, two samples from the diamict/glacimarine deposit dated to mid Younger Dryas 12,532 years B.P. and 12,660 years B.P., respectively (Figure 3 and Table 1). However, the reservoir age for this time period was higher than today [*Bondevik et al.*, 2006] and the sediments were most likely deposited during the Younger

©2014. American Geophysical Union. All Rights Reserved.

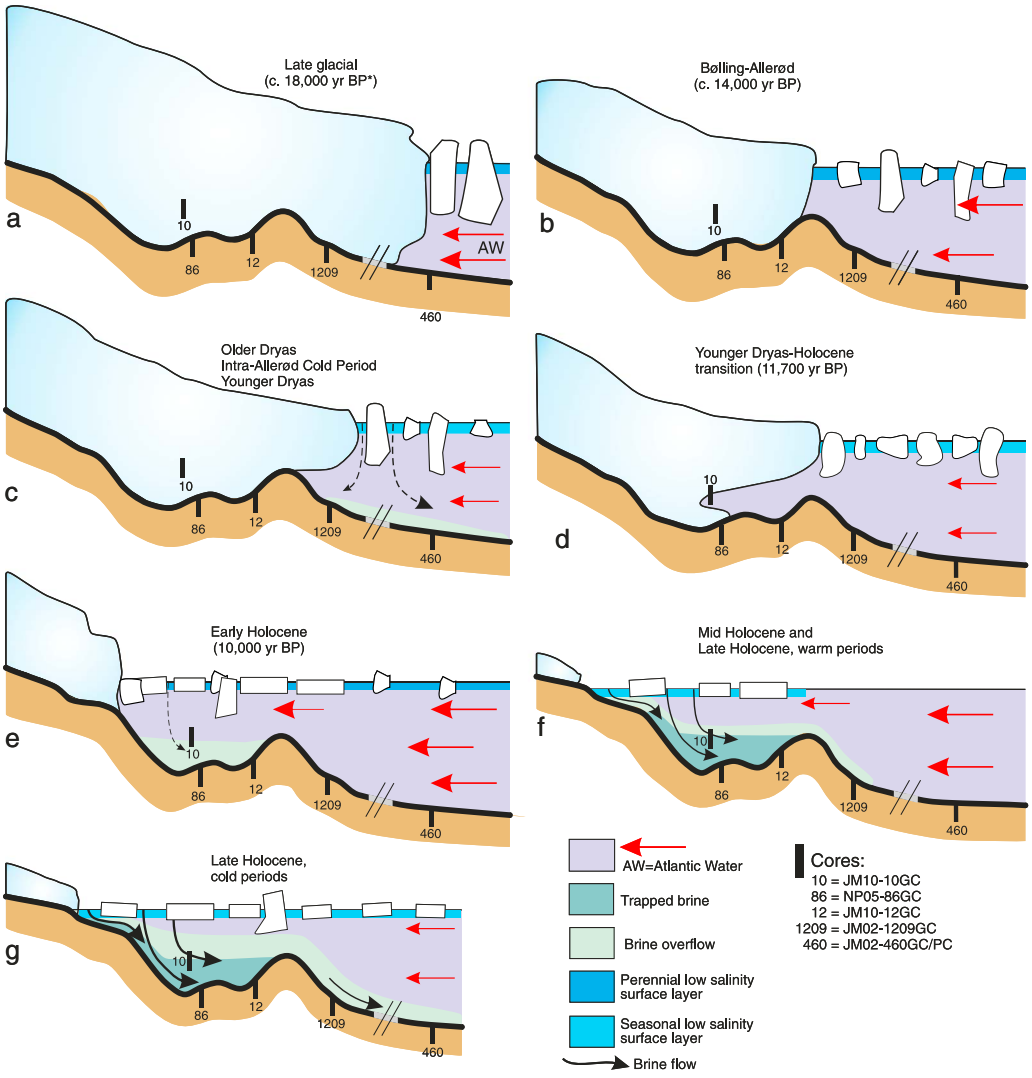

Figure 8. Schematic reconstruction of ice retreat and sea ice distribution, water mass movements, brine production, and brine distribution along a longitudinal section of Storfjorden for selected time intervals (see Figure 1b). (a) Late glacial period. (b) Bølling/Allerød warm interstadials. (c) Older Dryas/Intra-Allerød cold Phase/Younger Dryas cold events. (d) Younger Dryas-Holocene transition. (e) Early Holocene (until circa 8200). (f) Mid Holocene and late Holocene warm periods. (g) Late Holocene cold Periods.

Dryas-Holocene transition and represent the initial Holocene warming. Altogether, we conclude that most of the inner brine basin was filled with continental ice during the entire deglaciation, while the outer shelf and Storfjorden south of the sill were ice free (Figures 8b and 8c).

In the deglaciation records from core JM02-460GC from the outer shelf and core HH12-1209GC from Storfjorden, maxima in the percentage of agglutinated foraminifera coincide with the Older Dryas, the Intra-Allerød Cold Period, and the Younger Dryas stadial (Figures 5 and 6). These events are recognized as cold in the Greenland ice cores [*Cuffey and Clow*, 1997; *Alley*, 2000] (Figure 6) and in numerous other climate proxies from the Northern Hemisphere [e.g., *Lehman and Keigwin*, 1992; *Koç et al.*, 1993; *Björck et al.*, 1996]. On the western shelf of Svalbard the events are marked by a decreasing influence of Atlantic water and overall colder conditions [e.g., *Ślubowska et al.*, 2005; *Klitgaard Kristensen et al.*, 2013]. Storfjorden experienced a more extensive sea ice cover and increased brine production (Figure 8c) as indicated by the higher ratio of agglutinated to calcareous foraminifera and the lower percentage of $CaCO_3$ (Figures 5a, 5b, and 6). A similar correlation between the ratio of agglutinated to calcareous specimens and rapid climate shifts apparently

©2014. American Geophysical Union. All Rights Reserved.

occurred during the late Holocene circa 4000 years B.P. to the present. This time period is characterized by strongly fluctuating ratios (Figure 6), which in four of the five investigated cores (NP05-86GC, JM10-10GC, HH12-1209GC. and JM02-460GC) seem synchronous with climate shifts as indicated in the oxygen isotope record of the Greenland Ice Sheet Project (GISP) ice core and in sea surface temperature estimated on the basis of marine core 23258 from the slope southwest of Svalbard (Figure 6). This core contains the most detailed late Holocene sea surface temperature record from the Svalbard area [*Sarnthein et al*., 2003]. In cores NP05-86GC, JM10-10GC, HH12-1209GC, and JM02-460GC, high percentages of agglutinated foraminifera occur within the time intervals of circa 3200–2600, 2000–1600, 1500–1100, and 600–100 years B.P. coinciding, approximately, with cold periods in the ice core and in marine core 23258 (Figure 6). Some of the periods correlate with well-known cold intervals in the climate of northern Europe, for example, the Little Ice Age circa 600–100 years B.P. and the Dark Ages Cold Period circa 1500–1100 years B.P. [*Lamb*, 1965]. The intervening periods dominated by calcareous foraminifera correlate with the Roman Warm Period circa 2500–2000 years B.P. and the Medieval Warm Period circa 1000–700 years B.P. [*Lamb*, 1965]. In core JM10-12GC, taken close to the sill between the inner brine basin and the shelf, the fluctuations are partially offset from the pattern described above (Figure 6). This deviation may be due to discrepancies in the age models. JM10-12GC has fewer dating points than the other investigated cores (Figures 3 and 4).

In the late Holocene part of core JM02-460GC, the intervals dominated by agglutinating species are marked by higher percentages of TOC and apparently also by lower percentages of $CaCO_3$. The intervals dominated by agglutinating species are further characterized by higher percentages of fragmentation as demonstrated in cores HH12-1209GC and JM10-10GC (Figures 5a, 5b, and 7). The low percentages of $CaCO_3$ probably reflect the low proportion of calcareous foraminifera and therefore are in all probability mainly due to dissolution. The higher content of TOC probably reflects increasing organic productivity. In the Barents Sea, high productivity characteristically occurs along the Arctic Front (e.g., between Atlantic and Arctic water), in polynya, and at the sea ice edge (see above). It seems likely that the zone of seasonal sea ice was expanded during the Little Ice Age and other cold periods allowing for more polynyal activity and an enhanced brine production (Figures 8f and 8g). We note that the correlation between the percentage of TOC and climate varied oppositely during the deglaciation (Figure 5b). Here the content of TOC is highest in the warm intervals. The reason for this difference is not fully understood, but the environmental conditions during the two periods were very different. The overall conditions were colder with more extensive ice cover during the deglaciation, especially in the cold periods [see *Birgel and Hass*, 2004; *Müller et al*., 2009]. In general, the productivity was much lower during the deglaciation than at present.

The earliest Holocene period 11,700–circa 8200 years B.P. are in all the investigated cores distinguished by a strong dominance of calcareous foraminifera pointing to low brine production (Figures 5a and 5b). There are several possible explanations of this development. During the early Holocene the subsurface water along the western margin of Svalbard was dominated by the Atlantic water, which reached a Holocene temperature maximum between circa 11,300 and 8200 years B.P. [see *Rasmussen et al*., 2014b, and references therein]. The warm Atlantic water caused a massive melting of the Svalbard ice sheet. The result was a freshening of the coastal surface water and perennial stratification in Storfjorden and over the shelf (Figure 8e). We suggest that the low-saline surface water and a stratified water column was the cause for the apparently low brine production and low organic production during the early Holocene. The constantly high $\delta^{18}O$ values in NP05-86GC indicate that the deepest part of the inner basin throughout the Holocene has been filled with cold, salty bottom water probably originating from brines [*Rasmussen and Thomsen*, 2009] (Figures 5a and 8e–8g).

The high ratio of agglutinated to calcareous foraminifera in the early to mid-Holocene sediments is more difficult to interpret. In the brine basin, the percentage of agglutinated foraminifera increases from about 8200 years BP reaching a maximum around 5000 years BP (Figures 5a, 5b and 6). The concentration of agglutinated specimens remains almost constant throughout this period signifying that the increase in the percentage of agglutinated specimens is almost entirely caused by a decrease in the relative abundance and concentration of calcareous forms (Figure 5) The higher percentages of agglutinated foraminifera in the brine basin from circa 8200 years B.P. point to an increase in brine production. The reason for this could be a decrease in meltwater production bringing an end to the stratification (Figures 8f and 8g).

©2014. American Geophysical Union. All Rights Reserved.

The difference in brine intensity between the inner brine basin and outer trough is also reflected in the oxygen isotope values, which for the last 8000 years ranges from an average of 4.45‰ in NP05-86GC in the central brine basin to 4.25‰ in core JM10-12GC at the sill and to 4.10‰ in JM02-460GC on the shelf (Figures 5a and 5b). The gradually increasing isotope values in core JM02-460GC probably reflect a continuous cooling of the bottom water and increased brine activity [see *Duplessy et al*., 2005; *Rasmussen et al*., 2007; *Rasmussen and Thomsen*, 2009]. Core JM10-12GC shows increasing values until circa 8200 years B.P. and thereafter constant values as in NP05-86GC indicating minimal environmental change during most of the Holocene. Due to poor preservation of calcareous specimens in intervals dominated by agglutinated forms, the late Holocene isotope records from the brine basin are of low resolution and unable to resolve the rapid late Holocene fluctuations reflected in the foraminiferal faunas. Preservation is better in core JM02-460GC from the shelf, and here we observe a slight tendency for higher δ^{13}C values during cold periods dominated by agglutinated forms (Figures 5b and 7). However, the correlation is tentative and needs confirmation by studies of higher resolution.

The overall trend shown by the δ^{13}C records of JM02-460GC is similar to the trend shown by other δ^{13}C records of subsurface Atlantic Water from the western shelf of Svalbard with increasing values during the early and mid-Holocene and decreasing values during the late Holocene [see *Rasmussen and Thomsen*, 2009; *Jessen et al*., 2010; *Werner et al*., 2013; *Rasmussen et al*., 2014b] (Figure 5b). The δ^{13}C records from inside the brine basin differ from the shelf records by showing a continuing increase throughout the mid and late Holocene indicating a small but constant increase in ventilation (Figure 5a). We suggest that the improved ventilation in the brine basin is related to the increased production of well-oxygenated brines. Decrease in brine formation and ventilation occurred after the Little Ice Age (Figures 5a, 5b, and 8).

6. Conclusions

We have reconstructed brine formation in Storfjorden, Svalbard, in relation to climate changes and retreat of continental ice over the last circa 15,000 years B,P. Today, Storfjorden constitutes a unique marine environment with intense brine formation. The brines are cold, O_2 and CO_2 rich and often dense enough to reach the deep slope.

The study is based on five cores following the path of brines from their origin in the brine basin in the inner fjord to the time they leave the shelf and disappear into deep water. We have analyzed the relative abundance of calcareous versus agglutinated benthic foraminifera, degree of fragmentation of calcareous benthic foraminifera, the content of calcium carbonate and total organic carbon in the sediments, and oxygen and carbon isotopes.

The results indicate that in Storfjorden the ratio of agglutinated to calcareous foraminifera can be taken as an indication of the influence of brines in the area. Modern observations show that brines are very corrosive to calcareous tests, while at the same time they may act to preserve many agglutinated forms. These studies are supported by the fragmentation records from Storfjorden, which show a positive correlation between the percentage of fragmentation of calcareous specimens and the relative abundance of agglutinating forms.

Peaks in the relative abundance of agglutinated foraminifera indicate that brine production increased during the Older Dryas, the Intra-Allerød Cold Period, and the Younger Dryas cold interval and decreased during the Bølling and Allerød interstadials. Between 11,700 and circa 8200 years B.P., the faunas were totally dominated by calcareous species suggesting low brine production. After 8200 years B.P. the proportion of agglutinated specimens rose and from circa 4000–3000 years B.P. to recent the faunal composition shifted repeatedly between faunas dominated by agglutinated forms and faunas dominated by calcareous forms. Periods dominated by calcareous species, signifying low brine production, correlate with the Roman Warm Period circa 2500–2000 years B.P. and the Medieval Warm Period circa 1000–700 years B.P. Dominance of agglutinated species, signifying high brine production, occurred from 4000–2500 to 2000–1600 years B.P. and during the Dark Ages Cold Period 1500–1100 years B.P. and the Little Ice Age 600–100 years B.P.

©2014. American Geophysical Union. All Rights Reserved.

Acknowledgments
The study was financed by the University of Tromsø, the Mohn Foundation (Paleo-CIRCUS project), and the Norwegian Research Council (OA-Ocean Acidification project, grant 216538 and Centre of Excellence grant 223259). Parts of the study were also supported by Statoil and the Norwegian Polar Institute. The isotopes of JM10-12GC were measured at Bjerknes Centre, University of Bergen under the supervision of U. Ninnemann. I. Pathirana and J. Knies (Geological Survey of Norway, NGU) are thanked for contributing the measurements of magnetic susceptibility and some of the dates on core JM10-10GC. We thank N. Koç, and T.I. Karlsen (Norwegian Polar Institute) for the CTD data from August 2005. Bent Odgaard assisted with the statistical analysis. We also thank the crews of RV *Lance*, the Norwegian Polar Institute and RV *Jan Mayen* (now RV *Helmer Hanssen*), the University of Tromsø for their high-precision work retrieving cores from Storfjorden in mostly stormy conditions. Three reviewers, S. Korsun and two anonymous reviewers are thanked for helpful and constructive comments that greatly improved the manuscript. The data are uploaded to www.pangaea.de and are also available upon request to the corresponding author (tine.rasmussen@uit.no).

References

Alley, R. B. (2000), The Younger Dryas cold interval as viewed from central Greenland, *Quat. Sci. Rev.*, *19*, 213–226.

Alve, E., and J. W. Murray (1995), Experiments to determine the origin and palaeoenvironmental significance of agglutinated assemblages, in *Proceedings of the Fourth International Workshop on Agglutinated Foraminifera (Krakow, Poland), September 12–19, 1993*, *Spec. Publ.*, vol. 3, edited by M. A. Kaminski, S. Geroch, and M. A. Gasinski, pp. 1–11, Grzybowski Foundation, Krakow, Poland.

Alve, E., J. W. Murray, and J. Skei (2011), Deep-sea benthic foraminifera, carbonate dissolution and species diversity in Hardangerfjord, Norway: An initial assessment, *Estuarine Coastal Shelf Sci.*, *92*, 90–102.

Anderson, J. B. (1975a), Ecology and distribution of foraminifera in the Weddell Sea of Antarctica, *Micropaleontology*, *21*, 69–96.

Anderson, J. B. (1975b), Factors controlling $CaCO_3$ dissolution in the Weddell Sea from foraminiferal distribution patterns, *Mar. Geol.*, *19*, 315–332.

Anderson, L. G., E. P. Jones, R. Lindegren, B. Rudels, and P.-I. Sehlstedt (1988), Nutrient regeneration in cold, high salinity bottom water of the Arctic shelves, *Cont. Shelf Res.*, *8*, 1345–1355.

Anderson, L. G., E. Falck, E. P. Jones, S. Jutterström, and J. H. Swift (2004), Enhanced uptake of atmospheric CO_2 during freezing of seawater: A field study in Storfjorden, Svalbard, *J. Geophys. Res.*, *109*, C06004, doi:10.1029/2003JC002120.

Anderson, L. G., T. Tanhua, G. Björk, S. Hjalmarsson, E. P. Jones, S. Jutterström, B. Rudels, J. H. Swift, and I. Wåhlström (2010), Arctic Ocean shelf–basin interaction: An active continental shelf CO_2 pump and its impact on the degree of calcium carbonate solubility, *Deep Sea Res., Part I*, *57*, 869–879.

Arrigo, K. R., G. van Dijken, and M. Long (2008), Coastal Southern Ocean: A strong anthropogenic CO_2 sink, *Geophys. Res. Lett.*, *35*, L21602, doi:10.1029/2008GL035624.

Belyaeva, N. V., and I. I. Burmistrova (2003), Planktonic foraminifera in the Recent sediments of the Sea of Ohotsk, *Oceanology*, *43*, 206–214.

Berger, W. H., M.-C. Bonneau, and F. L. Parker (1982), Foraminifera on the deep-sea floor: Lysocline and dissolution rate, *Oceanol. Acta*, *5*, 249–258.

Birgel, D., and H. C. Hass (2004), Ocean and atmospheric variations during the last deglaciation in the Fram Strait (Arctic Ocean): A coupled high-resolution organic-geochemical and sedimentological study, *Quat. Sci. Rev.*, *23*, 29–47.

Björck, S., et al. (1996), Synchronised terrestrial-atmospheric records around the North Atlantic, *Science*, *274*, 1155–1160.

Bondevik, S., J. Mangerud, H. H. Birks, S. Gulliksen, and P. Reimer (2006), Changes in North Atlantic radiocarbon reservoir ages during the Allerød and Younger Dryas, *Science*, *312*, 1514–1517.

Cadman, V. (1996), Glaciomarine sedimentation and environments during the Late Weichselian and Holocene in the Bellsund Trough and Van Keulenfjorden, Svalbard, PhD thesis, Univ. of Cambridge, U. K., 250 pp.

Chierici, M., and A. Fransson (2009), Calcium carbonate saturation in the surface water of the Arctic Ocean: Undersaturation in freshwater influenced shelves, *Biogeosciences*, *6*, 2421–2432.

Commeau, R. F., L. A. Reynolds, and C. W. Poag (1985), Elemental X-ray mapping of agglutinated foraminifer tests: A non-destructive technique for determining compositional characteristics, *Micropaleontology*, *31*, 380–386.

Conan, S. M. -H., E. M. Ivanova, and G. -J. A. Brummer (2002), Quantifying carbonate dissolution and calibration of foraminiferal dissolution indices in the Somali Basin, *Mar. Geol.*, *182*, 325–349.

Cuffey, K. M., and G. D. Clow (1997), Temperature, accumulation, and ice sheet elevation in central Greenland through the last deglacial transition, *J. Geophys. Res.*, *102*, 26,383–26,396, doi:10.1029/96JC03981.

Damm, E., U. Schauer, B. Rudels, and C. Haas (2007), Excess of bottom-released methane in an Arctic shelf sea polynya in winter, *Cont. Shelf Res.*, *27*, 1692–1701.

Delille, B., B. Jourdain, A. V. Vieira Borges, J.-L. Tison, and D. Delille (2007), Biogas (CO_2, O_2, dimethylsulfide) dynamics in spring Antarctic fast ice, *Limnol. Oceanogr.*, *52*, 1367–1379.

Denne, R. A., and B. K. Sen Gupta (1989), Effects of taphonomy and habitat on the record of benthic foraminifera in modern sediments, *Palaios*, *4*, 414–423.

Duplessy, J. C., E. Cortijo, E. Ivanova, T. Khusid, L. Labeyrie, M. Levitan, I. Murdmaa, and M. Paterne (2005), Paleoceanography of the Barents Sea during the Holocene, *Paleoceanography*, *20*, PA4004, doi:10.1029/2004PA001116.

Fairbanks, R. G. (1989), A 17,000-years glacio-eustatic sea level record: Influence of glacial melting rates on the Younger Dryas event and deep-ocean circulation, *Nature*, *342*, 637–742.

Feely, R. A., S. C. Doney, and S. R. Cooley (2009), Ocean acidification: Present conditions and future changes in a high-CO_2 world, *Oceanography*, *22*, 36–47.

Fer, I., R. Skogseth, P. M. Haugan, and P. Jaccard (2003), Observations of the Storfjorden overflow, *Deep Sea Res., Part I*, *50*, 1283–1303.

Fransson, A., M. Chierici, P. L. Yager, and W. O. Smith Jr. (2011), Antarctic sea ice carbon dioxide system and controls, *J. Geophys. Res.*, *116*, C12035, doi:10.1029/2010JC006844.

Gooday, A. J. (1994), The biology of deep-sea foraminifera: A review of some advances and their applications in paleoceanography, *Palaios*, *9*, 14–31.

Gooday, A. J., and D. Claugher (1989), The genus Bathysiphon (Protista, Foraminiferida) in the northeast Atlantic: SEM observations on the wall structure of seven species, *J. Nat. History*, *23*, 591–611.

Haarpainter, J., J. C. Gascard, and P. M. Haugan (2001), Ice production and brine formation in Storfjorden, Svalbard, *J. Geophys. Res.*, *106*, 14,001–14,013, doi:10.1029/1999JC000133.

Hald, M., and P. I. Steinsund (1992), Distribution of surface sediment benthic foraminifera in the southwestern Barents Sea, *J. Foraminiferal Res.*, *22*, 347–362.

Hald, M., and P. I. Steinsund (1996), Benthic foraminifera and carbonate dissolution in the surface sediments of the Barents and Kara Seas, *Berichte zur Polarforschung*, *212*, 285–307.

Hald, M., H. Ebbesen, M. Forwick, F. Godtliebsen, L. Khomenko, S. Korsun, L. R. Olsen, and T. O. Vorren (2004), Holocene paleoceanography and glacial history of the West Spitsbergen area, Euro-Arctic margin, *Quat. Sci. Rev.*, *23*, 2075–2088.

Hebbeln, D., and H. Berner (1993), Surface sediment distribution in the Fram Strait, *Deep Sea Res., Part I*, *40*, 1731–1745.

Hebbeln, D., R. Henrich, and H.-.H. Baumann (1998), Paleoceanography of the last interglacial/glacial cycle in the Polar North Atlantic, *Quat. Sci. Rev.*, *17*, 125–153.

Hedley, R. H. (1963), Cement and iron in the areanceaous foraminifera, *Micropaleontology*, *9*, 433–441.

Ishman, S. E., and K. M. Foley (1996), Modern benthic foraminifer distribution in the Amerasian Basin, Arctic Ocean, *Micropalaeontology*, *42*, 206–220.

©2014. American Geophysical Union. All Rights Reserved.

Jessen, S. P., T. L. Rasmussen, T. Nielsen, and A. Solheim (2010), A new Late Weichselian and Holocene marine chronology for the western Svalbard slope 30,000–0 cal years BP, *Quat. Sci. Rev.*, *29*, 1301–1312.
Johannessen, O. M. (1987), Introduction: Summer Marginal Ice Zone Experiment during 1983 and 1984 in Fram Strait and the Greenland Sea, *J. Geophys. Res.*, *92*, 6716–6718, doi:10.1029/JC092iC07p06716.
Kelley, J. (1968), Carbon dioxide in the seawater under the Arctic Ice, *Nature*, *218*, 862–865.
Klitgaard Kristensen, D., T. L. Rasmussen, and N. Koç (2013), Paleoceanographic changes in the northern Barents Sea during the last 16,000 years—New constraints on the last deglaciation of the Svalbard-Barents Sea Ice Sheet, *Boreas*, *42*, 798–813.
Koç, N., E. Jansen, and H. Haflidason (1993), Paleoceanographic reconstructions of surface ocean conditions in the Greenland, Iceland and Norwegian seas through the last 14 ka based on diatoms, *Quat. Sci. Rev.*, *12*, 115–140.
Korsun, S., and M. Hald (1998), Modern benthic foraminifera off Novaya Zemlya tidewater glaciers, Russian Arctic, *Arct. Alp. Res.*, *30*, 61–77.
Kubischta, F., K. L. Knudsen, A. E. K. Ojala, and V.-P. Salonen (2011), Holocene benthic foraminiferal record from a high-Arctic fjord, Nordaustlandet, Svalbard, *Geografiska Ann. Ser. A, Phys. Geogr.*, *93*, 227–242.
Kuhnt, W., E. Collins, and D. B. Scott (2000), Deep water agglutinated foraminiferal assemblages across the Gulf Stream: Distribution patterns and taphonomy, in *Proccedings of the Fifth International Workshop on Agglutinated Foraminifera (Krakow, Poland), September 12–19, 1993*, *Spec. Publ.*, vol. 7, edited by M. B. Hart, M. A. Kaminski, and C. W. Smart, pp. 261–298, Grzybowski Foundation, Krakow, Poland.
Lamb, H. H. (1965), The early medieval warm period and its sequel, *Palaeogeogr. Palaeoclimatol. Palaeoecol.*, *1*, 13–37.
Le, J., and N. J. Shackleton (1992), Carbonate dissolution fluctuations in the western equatorial Pacific during the late Quaternary, *Paleoceanography*, *7*, 21–42, doi:10.1029/91PA02854.
Lehman, S. J., and L. D. Keigwin (1992), Sudden changes in North Atlantic circulation during the last deglaciation, *Nature, 356*, 757–762.
Li, B., H.-I. Yoon, and B.-K. Park (2000), Foraminiferal assemblages and $CaCO_3$ dissolution since the last deglaciation in the Maxwell Bay, King George Island, Antarctica, *Mar. Geol.*, *169*, 239–257.
Loeblich, A. R., and H. Tappan (1989), Implications of wall composition and structure in agglutinated foraminifers, *J. Paleontol.*, *63*, 769–777.
Loubere, P., and A. Gary (1990), Taphonomic process and species microhabitats in the living to fossil assemblage transition of deeper water benthic foraminifera, *Palaios*, *5*, 375–381.
Lubinski, D. J., L. Polyak, and S. L. Forman (2001), Freshwater and Atlantic water inflows to the deep northern Barents and Kara seas since ca 13 ^{14}C ka: Foraminifera and stable isotopes, *Quat. Sci. Rev.*, *20*, 1851–1879.
Lydersen, C., O. A. Nøst, P. Lovell, B. J. McConnell, T. Gammelsrød, C. Hunter, M. A. Fedak, and K. M. Kovacs (2002), Salinity and temperature structure of a freezing Arctic fjord—Monitored by white whales (*Delphinapterus leucas*), *Geophys. Res. Lett.*, *29*(23), 2119, doi:10.1029/2002GL015462.
Mackensen, A., and R. G. Douglas (1989), Down-core distribution of live and dead deep-water benthic foraminifera in box cores from the Weddell Sea and the California continental borderland, *Deep-Sea Res.*, *36*, 879–900.
Mackensen, A., H. Grobe, G. Kuhn, and D. K. Fütterer (1990), Benthic foraminiferal assemblages from the eastern Weddell Sea between 68 and 73°S: Distribution, ecology and fossilization potential, *Mar. Micropaleontol.*, *16*, 241–283.
Majewski, W., and M. Zajączkowski (2007), Benthic foraminifera in Adventfjorden, Svalbard, *J. Foraminiferal Res.*, *37*, 107–124.
Midttun, L. (1985), Formation of dense bottom water in the Barents Sea, *Deep-Sea Res.*, *32*, 1233–1241.
Müller, J., G. Massé, R. Stein, and S. T. Belt (2009), Variability of sea-ice conditions in the Fram Strait over the past 30,000 years, *Nat. Geosci.*, *2*, 772–776.
Murray, J. W. (2003), Foraminiferal assemblage formation in depositional sinks on the continental shelf west of Scotland, *J. Foraminiferal Res.*, *33*, 101–121.
Murray, J. W., and E. Alve (1999), Natural dissolution of shallow water benthic foraminifera: Taphonomic effects on the palaeocological record, *Palaeogeogr. Palaeoclimatol. Palaeoecol.*, *146*, 195–209.
Murray, J. W., and E. Alve (2011), The distribution of agglutinated foraminifera in NW European seas: Baseline data for the interpretation of fossil assemblages, *Palaeontol. Electron.*, *14*(2), 14A.
Nilsen, F., F. Cottier, R. Skogseth, and S. Mattsson (2008), Fjord-shelf exchanges controlled by ice and brine production: The interannual variation of Atlantic Water in Isfjorden, Svalbard, *Cont. Shelf Res.*, *28*, 1838–1853.
Omar, A., T. Johannessen, R. G. J. Bellerby, A. Olsen, L. G. Andersen, and C. Kivimàe (2005), Sea ice and brine formation in Storfjorden: Implications for the Arctic winter time air-sea CO_2 flux, in *Climate Variability in the Nordic Seas*, *Geophys. Monogr. Ser.*, vol. 158, edited by H. Drange et al., pp. 177–188, AGU, Washington, D. C.
Papadimitriou, S., H. Kennedy, G. Kattner, G. S. Dieckmann, and D. N. Thomas (2003), Experimental evidence for carbonate precipitation and CO_2 degassing during sea ice formation, *Geochim. Cosmochim. Acta*, *68*, 1749–1761.
Pathirana, I., J. Knies, M. Felix, and U. Mann (2013), Towards an improved organic carbon budget for the Barents Sea shelf, marginal Arctic Ocean, *Clim. Past Discuss.*, *9*, 4939–4986.
Pfuhl, H. A., and N. J. Shackleton (2004), Two proximal, high-resolution records of foraminiferal fragmentation and their implications for changes in dissolution, *Deep Sea Res., Part I*, *51*, 809–832.
Quadfazel, D., B. Rudels, and K. Kurtz (1988), Outflow of dense water from a Svalbard fjord into the Fram Strait, *Deep-Sea Res.*, *A35*, 1143–1150.
Rasmussen, S. O., et al. (2006), A new Greenland ice core chronology for the last glacial termination, *J. Geophys. Res.*, *111*, D06102, doi:10.1029/2005JD006079.
Rasmussen, T. L., and E. Thomsen (2009), Stable isotopes as signals of brines in the Barents Sea: Implications for brine formation during the last glaciation, *Geology*, *37*, 903–906.
Rasmussen, T. L., E. Thomsen, M. A. Ślubowska, S. Jessen, A. Solheim, and N. Koç (2007), Paleoceanographic evolution of the SW Svalbard margin (76°N) since 20,000 ^{14}C yr BP, *Quat. Res.*, *67*, 100–114.
Rasmussen, T. L., M. Forwick, and A. Mackensen (2012), Reconstruction of inflow of Atlantic Water to Isfjorden, Svalbard during the Holocene: Correlation to climate and seasonality, *Mar. Micropaleontol.*, *94–95*, 80–90.
Rasmussen, T. L., E. Thomsen, and T. Nielsen (2014a), Water mass exchange between the Nordic seas and the Arctic Ocean on millennial time scale during MIS 4–MIS 2, *Geochem. Geophys. Geosyst.*, *15*, 530–544, doi:10.1002/2013GC005020.
Rasmussen, T. L., E. Thomsen, K. Skirbekk, K. M. Ślubowska-Woldengen, D. Klitgaard Kristensen, and N. Koç (2014b), Spatial and temporal distribution of Holocene temperature maxima in the northern Nordic seas: Interplay of Atlantic-Arctic- and polar water masses, *Quat. Sci. Rev.*, *92*, 280–291.
Reigstad, M., J. Carroll, D. Slagstad, I. Ellingsen, and P. Wassmann (2011), Intra-regional comparison of productivity, carbon flux and ecosystem composition within the northern Barents Sea, *Prog. Oceanogr.*, *90*, 33–46.
Reimer, P. J., et al. (2013), IntCal13 and Marine13 radiocarbon age calibration curves, 0–50,000 years cal BP, *Radiocarbon*, *55*, 1869–1887.
Rudels, B., and D. Quadfasel (1991), Convection and deep water formation in the Arctic Ocean-Greenland Sea system, *J. Mar. Syst.*, *2*, 435–450.

©2014. American Geophysical Union. All Rights Reserved.

Rysgaard, S., R. N. Glud, M. K. Sejr, J. Bendtsen, and P. B. Christensen (2007), Inorganic carbon transport during ice growth and decay: A carbon pump in polar seas, *J. Geophys. Res.*, *112*, C03016, doi:10.1029/2006JC003572.
Sarnthein, M., S. van Kreveld, H. Erlenkeuser, P. M. Grootes, M. Kucera, U. Pflaumann, and M. Schulz (2003), Centennial-to-millennial-scale periodicities of Holocene climate and sediment injections off the western Barents shelf, 75°N, *Boreas*, *32*, 447–461.
Schauer, U. (1995), The release of brine-enriched shelf water from Storfjord into the Norwegian Sea, *J. Geophys. Res.*, *100*, 16,015–16,028, doi:10.1029/95JC01184.
Schell, T. M., T. J. Moss, D. B. Scott, and A. Rochon (2008), Paleo–sea ice conditions of the Amundsen Gulf, Canadian Arctic Archipelago: Implications from the foraminiferal record of the last 200 years, *J. Geophys. Res.*, *133*, JC03S02, doi:10.1029/2007JC004202.
Schröder, C. J. (1986), Deep-water areanaceous foraminifera in the northwest Atlantic Ocean, *Can. Tech. Rep. Hydrogr. Ocean Sci.*, *71*, 1–191.
Schröder, C. J. (1988), Subsurface preservation of agglutinated foraminifera in the Northwest Atlantic Ocean, *Abhandlungen der Geologischen Bundesantstalt*, *41*, 325–336.
Schröder-Adams, C. J., and D. van Rooyen (2011), Response of Recent benthic foraminiferal assemblages to contrasting environments in Baffin Bay and the nortern Labrador Sea Northwest Atlantic, *Arctic*, *64*, 317–341.
Scott, D. B., T. Schell, A. Rochon, and S. Blasco (2008), Benthic foraminifera in the surface sediments of the Beaufort Shelf and slope, Beaufort Sea, Canada: Applications and implications for past sea-ice conditions, *J. Mar. Syst.*, *74*, 840–863.
Sidner, B. R., and T. R. McKee (1975), Diagenesis of microfaunal remains from the Gyre Basin, in *Submarine Geomorphology and Sedimentation Patterns of the Gyre Intraslope Basin, Northwest Gulf of Mexico*, edited by A. H. Bouma, et al., pp. 132–140, Texas A & M Research Foundation, Tech. Rep., 75-9-T, College Station.
Skirbekk, K., D. Klitgaard Kristensen, T. L. Rasmussen, N. Koç, and M. Forwick (2010), Holocene climate variations at the entrance to a warm Arctic fjord: Evidence from Kongsfjorden Trough, Svalbard, in *Fjord Systems and Archives*, *Geol. Soc. London Spec. Publ.*, vol. 344, edited by J. A. Howe et al., pp. 291–306.
Skogseth, R., P. M. Haugan, and J. Haarpainter (2004), Ice and brine production in Storfjorden from four winters of satellite and in situ observations and modeling, *J. Geophys. Res.*, *109*, C10008, doi:10.1029/2004JC002384.
Skogseth, R., P. M. Haugan, and M. Jakobsson (2005a), Watermass transformations in Storfjorden, *Cont. Shelf Res.*, *25*, 667–695.
Skogseth, R., I. Fer, and P. M. Haugan (2005b), Dense-water production and overflow from an Arctic coastal polynya in Storfjorden, in *The Nordic Seas: An Integrated Perspective*, *Geophys. Monogr. Ser.*, vol. 158, edited by H. Drange, et al., pp. 73–88, AGU, Washington, D. C., doi:10.1029/158GM07.
Skogseth, R., L. H. Smedsrud, F. Nilsen, and I. Fer (2008), Observations of hydrography and downflow of brine-enriched shelf water in the Storfjorden polynya, Svalbard, *J. Geophys. Res.*, *113*, C08049, doi:10.1029/2007JC004452.
Ślubowska, M. A., N. Koç, T. L. Rasmussen, and D. Klitgaard Kristensen (2005), Changes in the flow of Atlantic Water into the Arctic Ocean since the last deglaciation: Evidence from the northern Svalbard continental margin, 80°N, *Paleoceanography*, *20*, *PA4014*, doi:10.1029/2005PA001141.
Ślubowska-Woldengen, M., T. L. Rasmussen, N. Koç, D. Klitgaard-Kristensen, F. Nilsen, and A. Solheim (2007), Advection of Atlantic Water to the western and northern Svalbard shelves through the last 17.5 ka cal yr BP, *Quat. Sci. Rev.*, *26*, 463–478.
Smethie, J. W., H. G. Østlund, and H. Loosli (1986), Ventilation of the deep sea: Evidence from Kr-85, tritium, C-14 and Ar-39, *Deep-Sea Res.*, *33*, 675–703.
Smith, S. L., W. O. Smith, L. A. Codispodi, and D. L. Wilson (1985), Biological observations in the marginal ice zone of the East Greenland Sea, *J. Mar. Res.*, *43*, 693–717.
Søgaard, D. H., D. N. Thomas, S. Rysgaard, R. N. Glud, L. Norman, H. Kaartokallio, T. Juul-Pedersen, and N. -X. Geilfus (2013), The relative contributions of biological and abiotic processes to carbon dynamics in subarctic sea ice, *Polar Biol.*, *36*, 1761–1777.
Stanford, J. D., E. J. Rohling, S. E. Hunter, A. P. Roberts, S. O. Rasmussen, E. Bard, J. McManus, and R. G. Fairbanks (2006), Timing of meltwater pulse 1a and climate responses to meltwater injections, *Paleoceanography*, *21*, PA4103, doi:10.1029/2006PA001340.
Steinsund, P. I. (1994), Benthic foraminifera in surface sediments of the Barents and Kara seas: Modern and late Quaternary applications, Phd thesis, Univ. of Tromsø, Tromsø, Norway, 111 pp.
Steinsund, P. I., and M. Hald (1994), Recent calcium carbonate dissolution in the Barents Sea, paleoceanographic applications, *Mar. Geol.*, *117*, 303–316.
Stuiver, M., and P. J. Reimer (1993), Extended ^{14}C database and revised CALIB radiocarbon calibration program, *Radiocarbon*, *35*, 215–230.
Van Aken, H. M., D. Quadfasel, and A. Warpakowski (1991), The Arctic Front in the Greenland Sea during February 1989: Hydrographic and biological observations, *J. Geophys. Res.*, *96*, 4739–4750, doi:10.1029/90JC02271.
Walter, L. M., and E. A. Burton (1990), Dissolution of recent platform carbonate sediments in marine pore fluids, *Am. J. Sci.*, *290*, 601–643.
Wassmann, P., D. Slagstad, C. Riser, and M. Reigstad (2006), Modelling the ecosystem dynamics of the Barents Sea including the marginal ice zone. II. Carbon flux and interannual variability, *J. Mar. Syst.*, *59*, 1–24.
Werner, K., R. F. Spielhagen, D. Bauch, H. C. Hass, and E. Kandiano (2013), Atlantic Water advection versus sea-ice advances in the eastern Fram Strait during the last 9 ka—Multiproxy evidence for a two-phase Holocene, *Paleoceanography*, *28*, 283–295, doi:10.1002/palo.20028.
Winkelmann, D., and J. Knies (2005), Recent distribution and accumulation of organic carbon on the continental margin west off Spitsbergen, *Geochem. Geophys. Geosyst.*, *6*, Q09012, doi:10.1029/2005GC000916.
Wollenburg, J. E., and W. Kuhnt (2000), The response of benthic foraminifera to carbon flux and primary production in the Arctic Ocean, *Mar. Micropaleontol.*, *40*, 189–231.
Wollenburg, J. E., A. Mackensen, and W. Kuhnt (2007), Benthic foraminiferal biodiversity response to a changing Arctic palaeoclimate in the last 24,000 years, *Palaeogeogr. Palaeoclimatol. Palaeoecol.*, *255*, 195–222.

©2014. American Geophysical Union. All Rights Reserved.